Fuzzy Uncertainty Analysis and Reliability Assessment of Aeroelastic Aircraft Wings

M. Rezaei, S. A. Fazelzadeh*
School of Mechanical Engineering
Shiraz University
Shiraz
Iran

A. Mazidi
School of Mechanical Engineering
Yazd University
Yazd
Iran

M. I. Friswell, H. H. Khodaparast
College of Engineering
Swansea University
Swansea
United Kingdom

ABSTRACT

In the present study, fuzzy uncertainty and reliability analysis of aeroelastic aircraft wings are investigated. The uncertain air speed and structural parameters are represented by fuzzy triangular membership functions. These uncertainties are propagated through the wing model using a fuzzy interval approach and the uncertain flutter speed is obtained as a fuzzy variable. Further, the reliability of the wing flutter is based on the interference area in the pyramid shape defined by the fuzzy flutter speed and air speed. The ratio between the safe region volume and the total volume

* S. A. Fazelzadeh, Tel: +98 7136133238; fax: +98 7136473511. E-mail address: Fazelzad@shirazu.ac.ir.

of the pyramid gives the reliability value. Two different examples are considered, a typical wing section and a clean wing, and the results are given for various wind speed conditions. The results show that the approach considered is a low-cost but suitable method to estimate the reliability of the wing flutter speed in the presence of uncertainties.
Keywords: Reliability; Uncertainty propagation; Fuzzy method; Aeroelastic aircraft; Wing flutter

NOMENCLATURE

$\mathbf{A}_{mat}$	State matrix
AC	Aerodynamic center
b	Mid-chord
$\mathbf{C_a}$	Aerodynamic damping matrix
$\mathbf{C_s}$	Structural damping matrix
$C_{L\theta}$	Lift curve slope
C_{gw}	Center of gravity
E	Elastic modulus
EA	Elastic axis
EI	Bending rigidity
G	Shear modulus
GJ	Torsional rigidity
I	Wing cross-sectional moment of inertia
I_P	Wing moment of inertia about P
J	Wing torsion constant
$\mathbf{K_a}$	Aeroelastic stiffness matrix
$\mathbf{K_s}$	Structural stiffness matrix
L	Aerodynamic lift
M	Aerodynamic moment
$\mathbf{M_a}$	Apparent mass matrix due to non-circulatory forces
$\mathbf{M_s}$	Inertia matrix
M_Q	Aerodynamic moment

R	Reliability
S	Flutter safety
U_F	Flutter speed
U	Air stream velocity
V	Volume of interference region
V_f	*Failure* Volume
V_s	Safe Volume
k_h	Flexural stiffness
k_θ	Torsional stiffness
l	Wing length
m	Typical section mass
w	Wing bending deflection
x_θ	Chord-wise offset of the center of mass from the reference point
χ	Possibility of each event
γ	Modal damping
λ	Eigenvalue
λ_0	Induced flow velocity
ρ	Air density
θ	Wing torsion deflection
ω	Modal frequency
ζ	Uncertain fuzzy parameter
$\mathbf{\Gamma}$	Modal damping vector
$\mathbf{\Lambda}$	Eigenvalues vector
$\mathbf{\Omega}$	Modal frequency vector
$\boldsymbol{\psi}$	State vector
$\boldsymbol{\xi}$	Generalized coordinate vector
$\boldsymbol{\zeta}$	Vector of uncertain fuzzy parameters

Subscripts

F	Flutter
c	crisp value – nominal value

f	failure region
s	safe region
min	minimum value
max	maximum value

1.0 INTRODUCTION

Flutter is an undesirable phenomenon which may take place in an aeroelastic wing. One way to predict the flutter speed is via theoretical calculations based on experimentally obtained wing parameters [2, 11, 49, 50, 56]. Most of these parameters are physically uncertain due to manufacturing and operational conditions. In general, uncertainties in flight vehicles are divided into two major categories: internal and external sources. Structural and geometric uncertainties are examples of internal uncertainties [18, 29, 30] and aerodynamic and gust loads are examples of external uncertainties [13, 14, 45].

Due to the lack of sufficient knowledge, the estimation of an appropriate model for the uncertain parameters is very important to estimate the flutter speed. Moreover, a reliability analysis is needed to determine the possibility of flutter failure; in this paper reliability is defined in terms of failure due to the flutter instability. Probabilistic and non-probabilistic methods are generally the two main approaches used for modeling uncertainties in structures. Probabilistic methods are based on generating a lot of data which leads to high cost calculations. Another problem with these methods is the lack of data that could be used to determine the statistical distribution of uncertain parameters. Non-probabilistic methods have been preferred in recent years due to their low-cost computations.

In this regard, the modeling of uncertain structures using a non-probabilistic interval method was conducted by Rao and Berke [43]. A non-traditional uncertainty treatment for mechanical problems was investigated by Muhanna and Mullen [34]. They introduced uncertainties as bounded possible values. Moreover, they modeled uncertainty with interval arithmetic and applied this method to beams and trusses. The numerical algorithms of non-probabilistic convex models and an interval method for the static displacement of structures with uncertain parameters was presented by Qiu [40]. Qiu and Wang [41] also investigated the non-probabilistic interval analysis method for the dynamical response of structures with interval parameters. Manson [27] used affine

and interval arithmetic to solve a two degrees of freedom eigenvalue problem. Qiu [42] also used an interval analysis method to predict the effect of uncertain-but-bounded parameters on the buckling of composite structures. Moens and Vandepitte [32] gave a review on the emerging non-probabilistic approaches for uncertainty treatment in finite element analysis. They discussed general theoretical and practical aspects of both interval and fuzzy finite element analysis. Muhanna et al. [35] combined the finite element method and interval analysis to analyze the system response subject to stiffness and loading uncertainties. The influence of uncertainty parameters using interval numbers on the flutter speed of a wing was conducted by Wang and Qiu [59]. They used a first-order Taylor series expansion to predict the lower and upper bounds of flutter speed. The problem of robust stability of a two dimensional nonlinear aeroelastic system with uncertainties using the μ-method was investigated by Yun and Hun [61]. The effect of parametric uncertainty on the stall flutter bifurcation behavior of a pitching airfoil was conducted by Sarkar et al. [46]. Khodaparast et al. [24] studied the problem of linear flutter analysis in the presence of uncertainties. The use of eigenvalue stability to analyse very large dimension aeroelastic numerical models arising from the exploitation of computational fluid dynamics has been reviewed by Badcock et al. [4]. Yang et al. [60] presented a new interval-based method for the analysis of uncertain structures using the Laplace transform. The upper and lower bounds of the natural frequencies of structures with uncertain but bounded parameters were evaluated by Sofi et al. [47]. They also applied improved interval analysis via an extra unitary interval (EUI).

Wang et al.[52] developed a sequential multidisciplinary design optimization and reliability analysis method under non-probabilistic theory to decouple the reliability analysis from the optimization. They also used an improved dimension-wise method for multidisciplinary interval uncertainty analysis [53].

Mannini and Bartoli [26] proposed a method to approach flutter instability and calculated the critical wind speed, starting from the probability distribution of the flutter derivatives. A probabilistic flutter analysis utilizing a meta-modeling technique to evaluate the effect of parameter uncertainty on the flutter speed was conducted by Abbas and Morgenthal [1]. Lokatt [25] approximated the aerodynamic model using a piece-wise continuous rational polynomial function. They proposed this method for efficient flutter analysis of aeroelastic systems including modelling uncertainties. Huan et al. [22] used the polynomial chaos expansion (PCE) method for uncertainty

quantification and showed that this method has less computational cost compared to Monte Carlo simulation.

Several other methods have been investigated to propagate uncertainty in mechanical structures. Friswell and Mottershead [18] described various methods for parameter selection, error localization, and sensitivity analysis and estimation, in mechanical structures. Also, many efforts were conducted on model updating in uncertain mechanical structures [7, 23, 28, 33]. The fuzzy approach has been used for uncertainty modeling and propagation, and this non-probabilistic method is computationally low-cost compared to probabilistic methods [48]. Chiang et al. [8] modeled structures with fuzzy and random uncertainties. They also studied the response of structures with stiffness, damping and mass uncertainties. A fuzzy methodology to calculate the eigenvalues and eigenvectors of an uncertain mechanical structure was proposed by Massa et al. [29]. They described material and geometric parameters as imprecise fuzzy numbers. De Gersem et al. [9] proposed the fuzzy finite element and interval methods to carry out frequency response and eigenvalue analysis of structures with uncertain parameters. The flutter dynamic pressure of a semi-span super-sonic wind-tunnel model was predicted by Tartaruga et al. [51]. They used probabilistic and non-probabilistic approaches in their study. Khodaparast et al. [20] presented the application of fuzzy finite element model updating to the DLR AIRMOD structure. Rezaei et al. [44] investigated the flutter uncertainty analysis of an aircraft wing subjected to a thrust force using a fuzzy method. They modeled the uncertain parameters as triangle and trapezium membership functions. The eigenvalue problem with fuzzy input parameters was solved using the fuzzy Taylor expansion method and a sensitivity analysis was performed. Also, the upper and lower bounds of the flutter region at different α-cuts were extracted. Wang et al.[54] proposed a new reliability estimation model based on the level cut strategy and volume ratio theory.

Although many researchers have studied uncertainty propagation and identification in structures, there are limited works in the field of reliability. The reliability and free vibration of a cantilever composite beam under structural uncertainty was conducted by Oh and Librescu [38]. The structural uncertainty was propagated using Monte Carlo Simulation and the Stochastic Rayleigh-Ritz method to find the reliability of the beam at different frequencies. Di Sciuva and Lomario [10] applied reliability methods to an isotropic beam and a laminated composite plate. Frangopoulos et al. [17] presented a review of life-cycle reliability optimization with an emphasis on aerospace and civil structures. Wang and Qiu [55] proposed a method to calculate the reliability

of an aeroelastic wing using an interval approach. Increasing the reliability of aircraft structures subject to air loads was conducted by Bijl et al. [5]. They also conducted some aeroelastic analysis and reliability studies to illustrate this key concept.

In this paper, uncertainty modeling is conducted using a possibility, rather than probability, approach. Possibility means something happens but with different quality, while probability means something happens or not. In conventional reliability, when the reliability of a system is 0.99, it means that if we have 100 systems, one of them may have failed on the defined criterion. In fuzzy reliability, when the reliability of a system is 0.99, it means that if we have 100 systems, none of them fail under the defined crierion but all of them have a 1% imperfection. Thus, fuzzy reliability speaks about the quality instead of quantity. The uncertain physical parameters are modeled as triangular fuzzy membership functions, although other membership functions, such as trapezoidal or Gaussian, may also be used. The uncertainty is then propagated through the aeroelastic wing model; a flutter analysis is conducted, and a fuzzy region of flutter is obtained instead of a deterministic flutter region. Furthermore, the reliability of the wing against flutter is determined from a pyramid based on the flutter speed and the air speed interference area.

To the best of the authors' knowledge, in the pertinent literature, the reliability of an aeroelastic wing using this type of fuzzy approach has not yet been presented. This research intends to fill the gap in knowledge related to this problem. In this paper, the stability region is presented as a three-dimensional fuzzy pyramid-shape. Furthermore, modal damping and frequency diagrams at different α-cuts are presented.

2.0 FLUTTER ANALYSIS OF A DETERMINISTIC WING MODEL

There are three general methods to estimate the wing flutter under unsteady aerodynamic loads, namely the K, PK and P methods [21]. The P method, including the finite state unsteady aerodynamic loading of Peters et al. [39], is most suited to the estimation of the flutter boundary [12, 16] and hence is used in this paper. In this method, the aeroelastic equations are converted to the state space form and the flutter boundary is obtained by solving an eigenvalue problem. The complex eigen solutions contain real and imaginary parts; by interpreting these values at different wind speeds, the flutter speed is determined from the stability of the eigenvalues.

The general discretized form of the wing aeroelastic governing equations can be expressed as:

$$\left(\mathbf{M}_s+\mathbf{M}_a\right)\ddot{\boldsymbol{\xi}}(t)+\left(\mathbf{C}_s+\mathbf{C}_a\right)\dot{\boldsymbol{\xi}}(t)+\left(\mathbf{K}_s+\mathbf{K}_a\right)\boldsymbol{\xi}(t)=\{\mathbf{O}\}, \tag{1}$$

where $\boldsymbol{\xi}$ is the generalized coordinates vector, $\mathbf{M_s}$ is the inertia matrix, $\mathbf{M_a}$ is the apparent mass matrix due to non-circulatory aerodynamic forces, $\mathbf{C_s}$ is the structural damping matrix, $\mathbf{C_a}$ is the aerodynamic damping matrix, $\mathbf{K_s}$ is the structural stiffness matrix and $\mathbf{K_a}$ is the aeroelastic stiffness matrix due to circularity forces [36, 37]. This second- order differential equation can be transformed into a set of first-order differential equations in state space:

$$\dot{\boldsymbol{\psi}}(\mathbf{t})=\mathbf{A_{mat}}\boldsymbol{\psi}(\mathbf{t}), \tag{2}$$

where the state vector $\boldsymbol{\psi}(\mathbf{t})$ is defined as:

$$\boldsymbol{\psi}(\mathbf{t})=\begin{bmatrix}\boldsymbol{\xi}(\mathbf{t})\\ \dot{\boldsymbol{\xi}}(\mathbf{t})\end{bmatrix}. \tag{3}$$

The system matrix $\mathbf{A_{mat}}$ is obtained as:

$$\mathbf{A_{mat}}=\begin{bmatrix}\mathbf{O} & \mathbf{I}\\ -\left(\mathbf{M}_s+\mathbf{M}_a\right)^{-1}\left(\mathbf{K}_s+\mathbf{K}_a\right) & -\left(\mathbf{M}_s+\mathbf{M}_a\right)^{-1}\left(\mathbf{C}_s+\mathbf{C}_a\right)\end{bmatrix}. \tag{4}$$

After solving equation (2), the eigenvalue vector is derived as

$$\boldsymbol{\Lambda}=\boldsymbol{\Gamma}\pm\mathbf{i}\,\boldsymbol{\Omega}, \tag{5}$$

where $\boldsymbol{\Gamma}$ is modal damping vector (with elements γ_j) and $\boldsymbol{\Omega}$ (with elements ω_j) is the modal frequency vector. When $\gamma_j<0$ for all j, any transient oscillations decay and the system is dynamically stable. As the wind speed increases, one component of the modal damping vector tends to zero and then becomes positive. The first airspeed at which this element become zero is the flutter speed and the corresponding modal frequency is the flutter frequency.

3.0 FUZZY UNCERTAINTY APPROACH

The wing flutter speed is generally an uncertain parameter because it depends upon structural and aerodynamic parameters which are physically uncertain due to manufacturing and operational

conditions. Airspeed is also not a certain parameter; when the speed is set at a specified value during the flight, the air speed may fluctuate around this value due to atmospheric conditions.

An eigenvalue problem for the P method including uncertain parameters, can be represented as [29]:

$$\dot{\boldsymbol{\psi}}(\mathbf{t}) = \mathbf{A}_{\mathbf{mat}}\left(\tilde{\zeta}_1, \tilde{\zeta}_2, ..., \tilde{\zeta}_m\right)\boldsymbol{\psi}(\mathbf{t}), \tag{6}$$

where the $\tilde{\zeta}_i$ are the uncertain parameters and m is the number of uncertain parameters. The uncertain parameters are modeled as fuzzy numbers. The fuzzy parameter $\tilde{\zeta}$, which is shown in Figure 1, is defined by a variation about a crisp value at each α-cut.

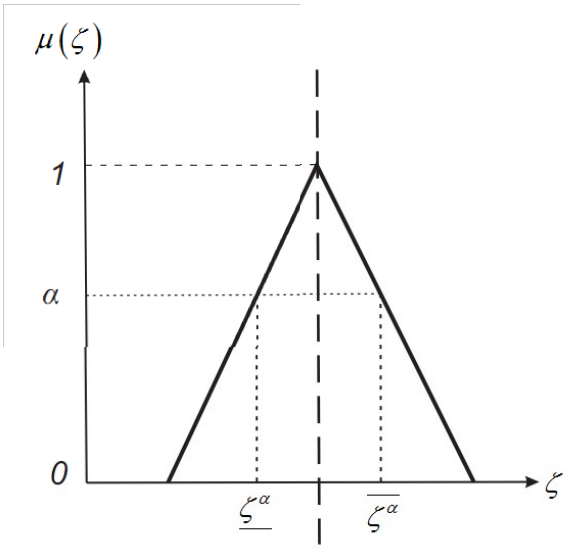

Figure 1. Triangular fuzzy membership function.

According to this figure, an α-cut is the set of all ζ such that $\mu(\zeta)$ is greater than or equal to α. The fuzzy vector $\tilde{\zeta}$ is defined by a crisp value ζ_c and the variation $\Delta\tilde{\zeta}$ at a given α-cut as

$$\tilde{\zeta}^{\alpha} = \zeta_c + \Delta\tilde{\zeta}^{\alpha}, \tag{7}$$

or

$$\tilde{\zeta}^{\alpha} = \xi_c + \left[\underline{\Delta\zeta^{\alpha}}; \overline{\Delta\zeta^{\alpha}}\right], \tag{8}$$

where $\overline{\zeta^{\alpha}}$ and $\underline{\zeta^{\alpha}}$ are the maximum and minimum of the fuzzy parameter vector $\tilde{\zeta}$ for a given α-cut, respectively. The membership function is discretized by different intervals which are linked to α-cuts ranging from 0 to 1.

Many methods to determine output (response) intervals based on the input (parameter) intervals are available, many of which use the exact input-output functional relationship. Here, to demonstrate the proposed approach, the interval is divided into several intervals at each α-cut and a first order Taylor series expansion is used to determine the upper and lower bounds of the flutter frequency and modal damping for each interval.

The interval model can be used to describe nonlinear dynamic systems under uncertainty with low-order Taylor series expansions. However, the Taylor series-based interval method is only suitable for problems with small uncertainty levels [58]. Truncation errors exist in this linear model since the higher-order terms are neglected, but for highly nonlinear problems, the truncation error cannot be ignored [57].

Using this method, the modal damping and frequency are expressed as

$$\gamma^{\alpha}\left(\zeta,U\right)=\gamma^{\alpha}\left(\zeta_{c},U\right)+\sum_{j=1}^{m}\left|\frac{\partial\gamma^{\alpha}\left(\zeta_{c},U\right)}{\partial\zeta_{i}^{\alpha}}\right|\Delta\zeta_{i}^{\alpha}, \tag{9}$$

$$\omega^{\alpha}\left(\zeta,U\right)=\omega^{\alpha}\left(\zeta_{c},U\right)+\sum_{j=1}^{m}\left|\frac{\partial\omega^{\alpha}\left(\zeta_{c},U\right)}{\partial\zeta_{i}^{\alpha}}\right|\Delta\zeta_{i}^{\alpha}, \tag{10}$$

After applying the interval operation, the lower and the upper bounds of the modal damping at each α-cut are defined, respectively, as:

$$\underline{\gamma^{\alpha}}\left(\zeta,U\right)=\gamma^{\alpha}\left(\zeta_{c},U\right)+\sum_{j=1}^{m}\left|\frac{\partial\gamma^{\alpha}\left(\zeta_{c},U\right)}{\partial\zeta_{i}^{\alpha}}\right|\underline{\Delta\zeta_{i}^{\alpha}}, \tag{11}$$

$$\overline{\gamma^{\alpha}}\left(\zeta,U\right)=\gamma^{\alpha}\left(\zeta_{c},U\right)+\sum_{j=1}^{m}\left|\frac{\partial\gamma^{\alpha}\left(\zeta_{c},U\right)}{\partial\zeta_{i}^{\alpha}}\right|\overline{\Delta\zeta_{i}^{\alpha}}, \tag{12}$$

Also, the lower bound and the upper bound of the modal frequency at each α-cut are:

$$\underline{\omega^{\alpha}}\left(\zeta,U\right)=\omega^{\alpha}\left(\zeta_{c},U\right)+\sum_{j=1}^{m}\left|\frac{\partial\omega^{\alpha}\left(\zeta_{c},U\right)}{\partial\zeta_{i}^{\alpha}}\right|\underline{\Delta\zeta_{i}^{\alpha}}\,, \tag{13}$$

$$\overline{\omega^{\alpha}}\left(\zeta,U\right)=\omega^{\alpha}\left(\zeta_{c},U\right)+\sum_{j=1}^{m}\left|\frac{\partial\omega^{\alpha}\left(\zeta_{c},U\right)}{\partial\zeta_{i}^{\alpha}}\right|\overline{\Delta\zeta_{i}^{\alpha}}\,, \tag{14}$$

Note that taking the absolute values of the sensitivities in equations (11) to (14) may lead to conservative bounds. The flutter speed that corresponds to equation (11) gives the upper bound of the flutter speed ($\underline{U_F^{\alpha}}$), and the flutter speed that corresponds to equation (12) provides the lower bound of the flutter speed ($\overline{U_F^{\alpha}}$). The crisp values can be easily obtained by solving equation (2). Analytical expressions of the partial derivatives $\partial\gamma^{\alpha}\left(\zeta_{c},U\right)/\partial\zeta_{i}^{\alpha}$ and $\partial\omega^{\alpha}\left(\zeta_{c},U\right)/\partial\zeta_{i}^{\alpha}$ cannot be obtained easily due to the complicated implicit functional relationship between γ and ω. One practical method to calculate these expressions is to use finite difference approximations [55]. After solving the above equations, the flutter speed bound at each α-cut is derived. These bounds are combined to achieve the example membership function shown in Figure 2.

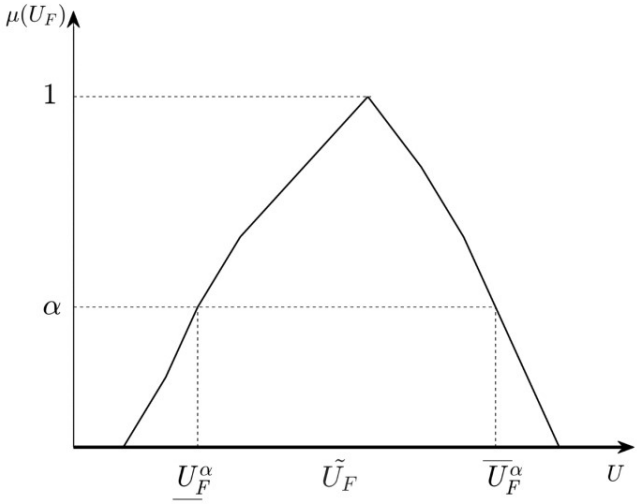

Figure 2. An example flutter speed membership function.

4.0 RELIABILITY OF THE WING FLUTTER SPEED

In this section, the reliability of the wing flutter speed is investigated. To this end, the flutter speed and air speed interference pyramid is obtained and then the fuzzy reliability approach is employed to determine the flutter reliability.

4.1. Airspeed and flutter speed interference

The method to obtain the flutter speed membership function was described in the previous section. The air speed can be modeled as another membership function $\widetilde{U_w}$. It is assumed that the crisp value of the air speed is U_w^{c}, and it will not be less than $U_w^{\min}$ nor greater than $U_w^{\max}$. If the triangular membership function is used for the air speed it means that the possibility of U_w^{c} is α=1. For other interval points, the possibility reduces linearly from 1 to 0. When the air speed is equal to $U_w^{\min}$ or lower, or when the air speed is equal to $U_w^{\max}$ or higher, the possibility of the air speed is zero. The possibility of the air speed membership function $\widetilde{U_w}$ can be written as:

$$\mu(U)=\begin{cases} 0 & U \le U_w^{\min} \\ \dfrac{U-U_w^{\min}}{U_w^{c}-U_w^{\min}} & U_w^{\min} < U < U_w^{c} \\ 1 & U = U_w^{c} \\ \dfrac{U-U_w^{\max}}{U_w^{\mathrm{c}}-U_w^{\max}} & U_w^{\mathrm{c}} < U < U_w^{\max} \\ 0 & U_w^{\max} \le U \end{cases} \tag{15}$$

The air speed and flutter speed membership functions and their two dimensional interference are shown in Figure 3.

If there is a region where this interference occurs, then there is a possibility of flutter, otherwise, the flutter possibility is zero. In this section, the flutter reliability of the wing is calculated based on the general non-probabilistic interval reliability model. Wang and Qiu [55] used this method for flutter reliability analysis by means of rectangular membership functions for flutter speed and air speed. They represented the flutter speed and air speed in a plane, as shown in Figure 4. The solid rectangle shows the region of variation of both $\widetilde{U_w}$ and $\widetilde{U_F}$. By crossing this region with the failure plane $U_w = U_F$, the safe region and the failure region can be determined as shown in Figure 4.

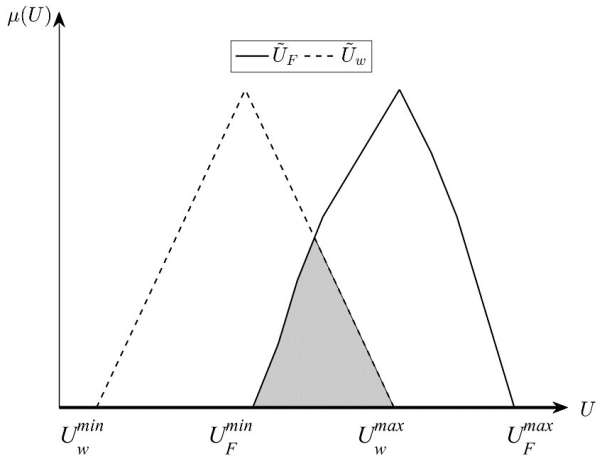

Figure 3. Flutter speed and wind speed 2-D fuzzy interference.

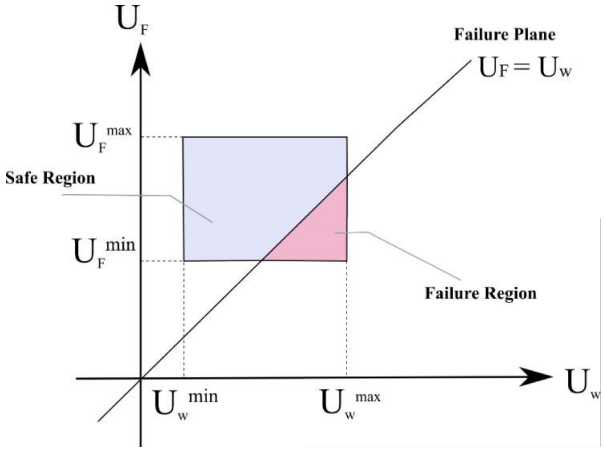

Figure 4. Space of variables and the occurrence of interference.

Here, due to the use of triangular membership functions for flutter speed and air speed, such a space of variables occurs at each α-cut. By assembling this space of variables at all α-cuts, a pyramid is created in the space of $U_w - U_F - \alpha$, as shown in Figure 5. The approach would also work for non-triangular membership functions although the shapes would be more complex and the computation more intensive.

This pyramid shows the region of variations of $\widetilde{U_w}$, and $\widetilde{U_F}$ for each α-cut. By cutting this volume with the failure plane $U_w = U_F$, the safe volume and the failure volume are defined as shown in Figure 6. Using this approach, the effects of both air speed and flutter speed uncertainties are considered in the reliability analysis.

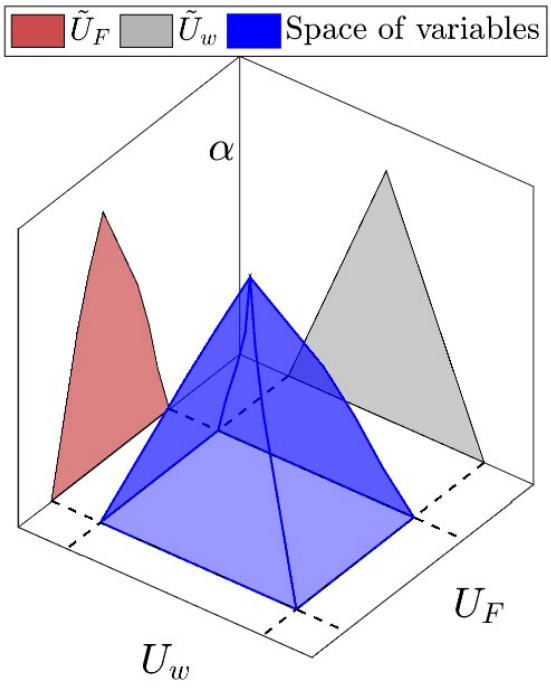

Figure 5. The pyramid of variables in the case of triangular membership functions.

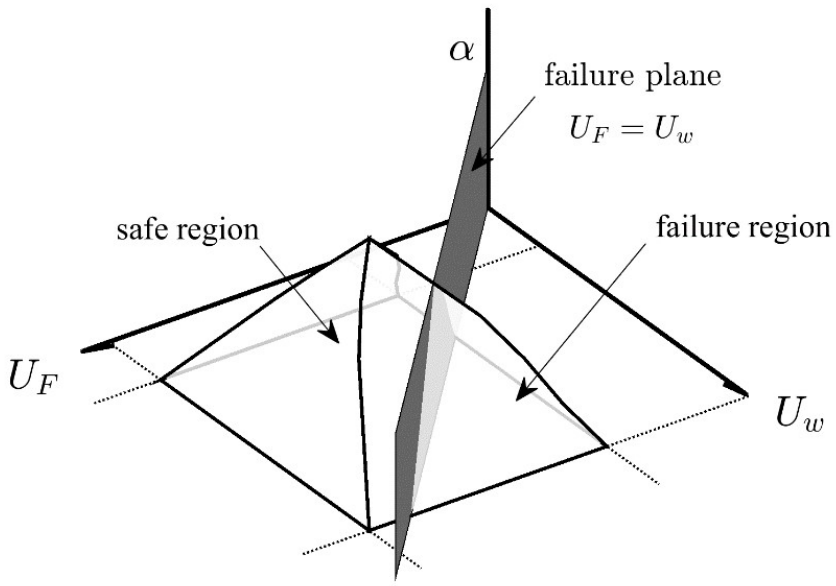

Figure 6. Safe region and failure region.

4.2. Fuzzy reliability of the wing flutter speed

In the design process, the air speed $\widetilde{U_w}$ is required to be smaller than the flutter speed $\widetilde{U_F}$. This implies that with respect to the crisp values (α=1), the wing should be safe. As a result of the dispersion of the fuzzy areas, they may share the same numerical values, shown in Figure 3 as the shaded region.

As shown before, the space of variables forms a pyramid. This volume is a function of U_w and U_F, and defined as $F_V\left(U_F,U_w\right)$. By integrating this function, the total volume of the space of variables is obtained as:

$$V=\iiint_V F_V\left(U_F,U_w\right)dV\,, \tag{16}$$

The integration of equation (16) is evaluated numerically. In this method the pyramid in the possible space is divided into cuboids based on the number of alpha cuts, as shown in Fig. 7 schematically. Then the volume of the pyramid is obtained by summing the volumes of all of the cuboids. To evaluate the failure volume, the cuboid for each α-cut is split into two polygon prisms (for example triangular prisms) defined by the failure plane. The volume of the failure region is obtained by summing the volume of all of the prisms within the failure region. .

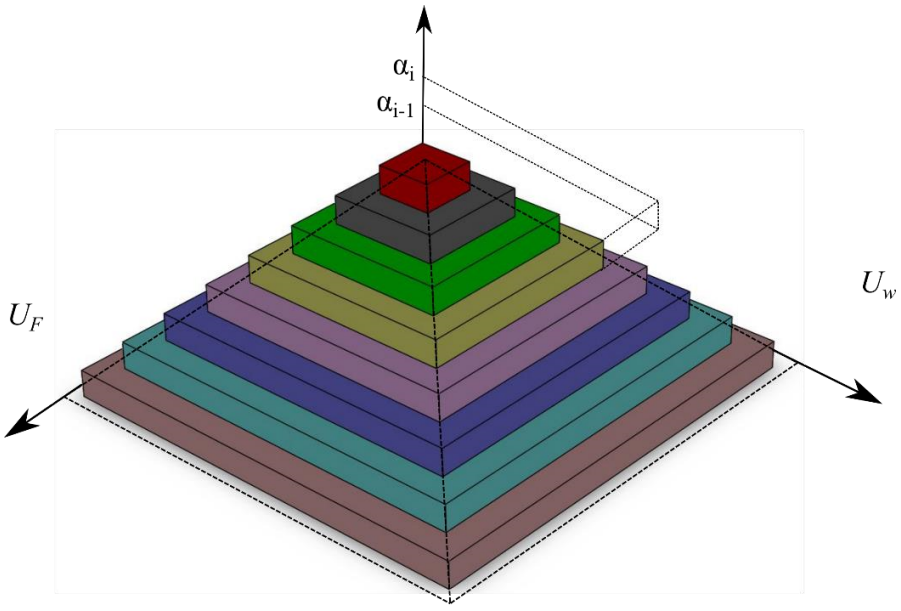

Figure 7. Numerical integration evaluation to obtain the volume of the possible space.

The safe volume V_s is the part of this total volume V in which $U_w \le U_F$, and the failure volume V_f is the part of the total volume V in which $U_w \ge U_F$ (see Figure 6). To present the mathematical concept, the following function is defined.

$$\Xi = \widetilde{U_F} - \widetilde{U_w}, \tag{17}$$

The safe volume is a volume in which $\Xi>0$ and the failure volume is a volume in which $\Xi<0$. For the case $\Xi=0$ the failure plane is created. Assuming that χ is the possibility of each event, the possibility of the safe region is obtained as:

$$\chi(\Xi<0)=\frac{V_s}{V}, \tag{18}$$

Similarly, the possibility of the failure region is:

$$\chi(\Xi>0)=\frac{V_f}{V}, \tag{19}$$

Then the reliability or safety probability of the flutter speed is formulated as:

$$R=\chi(\Xi<0)=\frac{V_s}{V}=1-\frac{V_f}{V}, \tag{20}$$

Figure 8 shows a case in which all parts of the space of variables are in the safe region. In this case, the flutter airspeed membership function lower bound is larger than the maximum wind speed and the reliability of the flutter occurrence is 1. This means that the flutter will not happen under any circumstances.

If all parts of the space of variables are located in the region where $\Xi = \widetilde{U_F} - \widetilde{U_w} > 0$, as shown in Figure 9, then the air speed is always larger than the maximum flutter airspeed. In this case, the reliability of flutter occurrence is 0, and hence flutter will definitely happen.

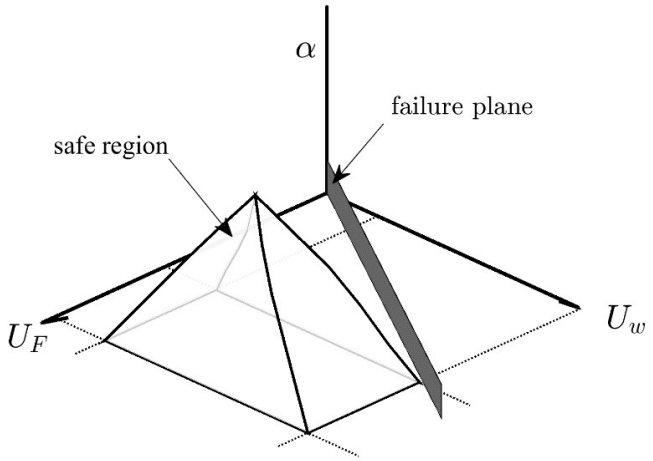

Figure 8. A case in which all parts of the interference volume are in the safe region.

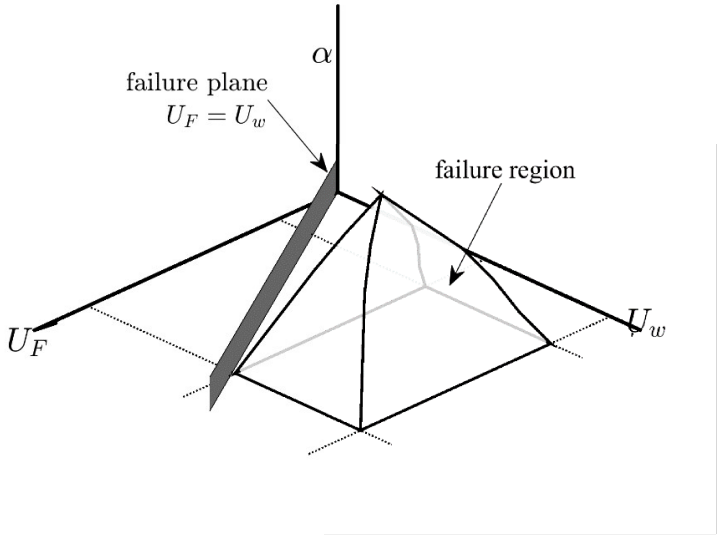

Figure 9. A case in which all parts of the interference volume are in the failure region.

The steps for this method are given as a flowchart in Figure 10. First, uncertain parameters are determined as fuzzy membership functions. Then these fuzzy membership functions are divided to intervals, and the intervals are evaluated at each value of α. In the next step, the interval corresponding to each α-cut is propagated into the structural equations using a Taylor series expansion, and the upper and lower bounds of the flutter speed are obtained. By assembling the flutter speed at each α-cut the flutter speed membership function is obtained. The 3D interference

between the obtained flutter speed and the airspeed membership functions forms a pyramid. By interpreting the volume of this pyramid by the mentioned cutting plane the flutter reliability is obtained.

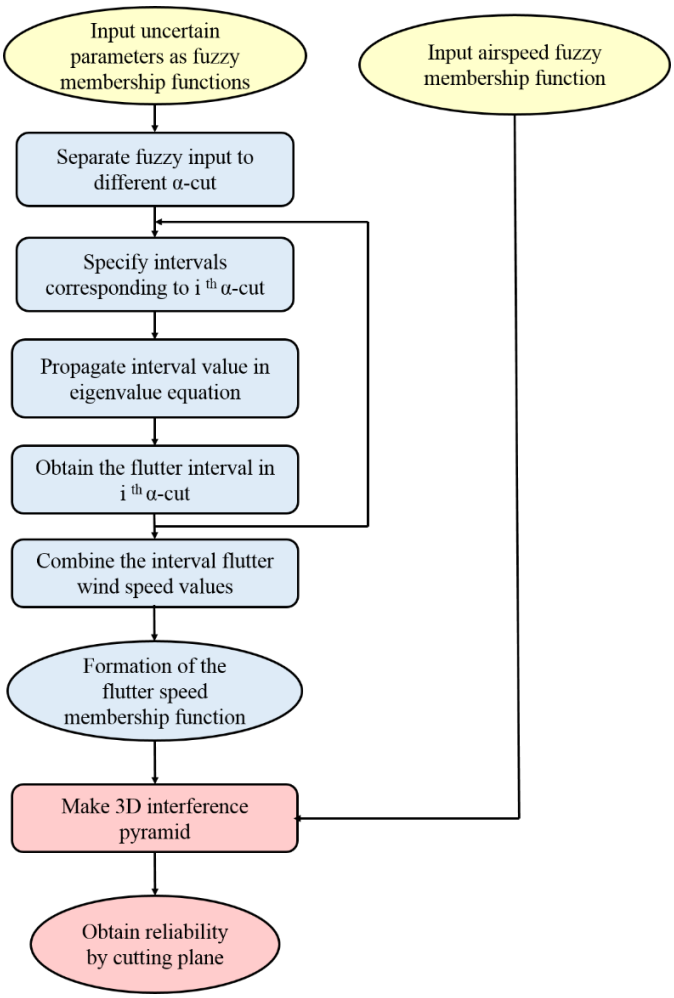

Figure 10. Fuzzy method flowchart

5.0 NUMERICAL EXAMPLES

Many theoretical and experimental studies on wing aeroelasticity have been performed in the literature using typical section models [3, 15]. These models can represent typical airfoil sections along a finite wing and are still widely used by researchers because of their simplicity. The most popular structural models used for wing aeroelasticity are beam models [16, 19, 31]. These models consider the wing as a flexible beam that experiences, in general, bending in two orthogonal planes

and torsion about the elastic axes. In this section, to illustrate the feasibility of the fuzzy reliability method, a typical section 2D wing model and a clean wing 3D model are used.

5.1. Example 1: Typical Section 2D Wing Model

A typical section wing model [21] is shown in Figure 11. This configuration could represent the case of a rigid, two-dimensional wind-tunnel model that is elastically mounted in a wind-tunnel test section, or could correspond to a typical airfoil section along a finite wing. In the latter case, the discrete springs would reflect the wing structural bending and torsional stiffness, and the reference point would represent the wing elastic axis.

Suppose that the wing mass, moment of inertia and flexural and torsional stiffnesses are uncertain parameters. These parameters should be converted to fuzzy triangle membership functions. The membership functions are expressed as (ξ_{min}, ξ_c, ξ_{max}) in which ξ_{min} and ξ_{max} are minimum and maximum values at α=0, and ξ_c is the value at α=1. The fuzzy triangle membership functions of the uncertain parameters are assumed to be $\overline{m} = (0.95m, m, 1.05m)$, $\overline{I_P} = (0.95I_P, I_P, 1.05I_P)$, $\overline{k_h} = (0.95k_h, k_h, 1.05k_h)$ and $\overline{k_\theta} = (0.95k_\theta, k_\theta, 1.05k_\theta)$.

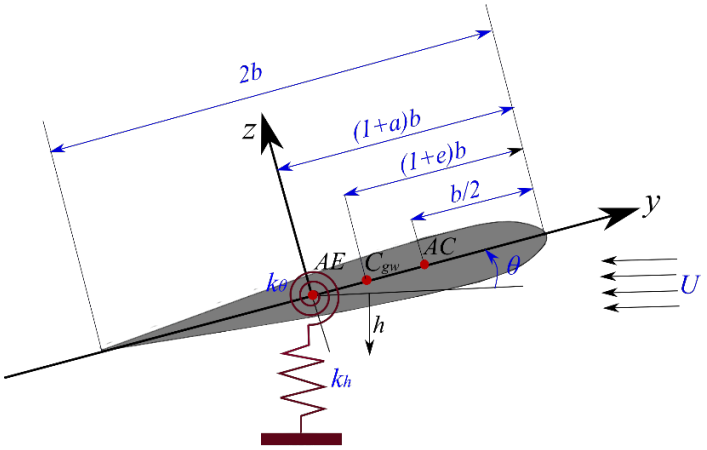

Figure 11. A typical section wing model.

The aeroelastic governing equations can be derived as:

$$m\left(\ddot{h} + bx_\theta\ddot{\theta}\right) + k_h h = -L, \tag{21}$$

$$I_P\ddot{\theta} + mbx_\theta\ddot{h} + k_\theta\theta = M_Q + b\left(\frac{1}{2} + a\right)L, \tag{22}$$

where m is the typical section mass, x_θ is the chord-wise offset of the center of mass from the reference point, I_P is the moment of inertia about P, L is the aerodynamic lift, M_Q is the aerodynamic moment and k_h and k_θ are flexural and torsional stiffnesses, respectively.

Unsteady aerodynamic loads are simulated based on the model of Peters et al. [39] as

$$L = \pi\rho b^2\left[\ddot{h} + U\dot{\theta} - ba\ddot{\theta}\right] + C_{L\theta}\rho U b\left[\dot{h} + U\theta + b\left(\frac{1}{2} - a\right)\dot{\theta} - \lambda_0\right], \tag{23}$$

$$M_Q = -\pi\rho b^3\left(\frac{1}{2}\ddot{h} + b\left(\frac{1}{8} - \frac{a}{2}\right)\ddot{\theta} + U\dot{\theta}\right), \tag{24}$$

where $\lambda_0 = \sum_{n=1}^{N} b_n\lambda_n$ is the induced flow velocity and is calculated through a system of N first order coupled differential equations [21].

To solve the above equations, the following dimensionless parameters are introduced.

$$r^2 = \frac{I_p}{mb^2} \quad \sigma = \frac{\omega_h}{\omega_\theta} \quad \mu = \frac{m}{\pi\rho b^2} \quad V = \frac{U}{b\omega_\theta}. \tag{25}$$

For validation, the modal damping versus dimensionless air speed is shown in Figure 12 and compared with the results given in reference [21]. This validation is performed to determine the accuracy of the current aeroelastic governing equations and the solution methodology.

Furthermore, for model validation, the deterministic typical section model is also compared with an Equivalent 2D Goland wing [19] in which the flexural and torsional stiffness are considered as $k_h = 0.597^4\left(\pi/L\right)^4 EI$ and $k_\theta = \left(\pi/2L\right)^2 GJ$. The parameters are given in Table 1. The flutter speed and frequency are obtained and compared in Table 2. The results show that this 2D model with finite state unsteady aerodynamic loading is in good agreement with the mentioned reference.

To obtain the flutter fuzzy membership function the dominant flutter mode is considered. In this example, the bending mode experiences flutter and the other modes are stable.

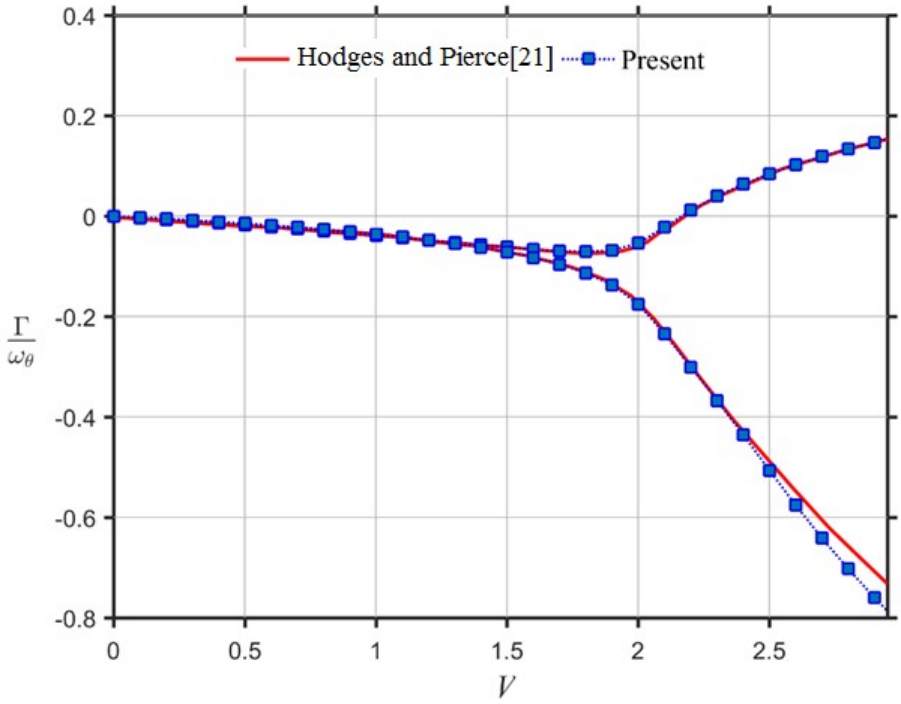

Figure 12. Modal damping versus dimensionless airspeed for a = -0.2, e = 0.1, μ = 20, r^2 = 0.24 and σ = 0.4.

Table 1
Goland wing parameters[6]

Parameters	Value	Unit
EI	9.77×10^6	N.m^2
GJ	9.890×10^5	N.m^2
l	6.09	m
x_θ	0.182	m
a	-0.333	
m	35.7187	kg/m
b	0.9144	m
r	0.457	m
k_θ	8.75×10^4	N/m
k_h	6.57×10^4	N/m
ρ	1.225	kg/m^3

Table 2
Deterministic flutter speed and frequency

Flutter speed (m/s)	Flutter frequency (rad/s)	Reference
137.09	71.36	Present 3D (Example 2)
140.73	73.21	Present 2D (Example 1)
141.17	72.56	Borello et al. 2D [6]
137.05	75.52	Fazelzadeh et al.3D [12]
137.16	70.69	Goland Exact [19]

Assuming that the relationship between the eigenvalues and the uncertain parameters is monotonic, and applying the fuzzy interval method, the modal damping for each α-cut is obtained as:

$$\begin{aligned}\overline{\gamma^{\alpha}}\left(m,I,k_h,k_\theta,U\right)&=\gamma^{\alpha}\left(m_c,I_c,k_{hc},k_{\theta c},U\right)+\left|\frac{\partial\gamma^{\alpha}\left(m_c,I_c,k_{hc},k_{\theta c},U\right)}{\partial m^{\alpha}}\right|\overline{\Delta m^{\alpha}}\\&+\left|\frac{\partial\gamma^{\alpha}\left(m_c,I_c,k_{hc},k_{\theta c},U\right)}{\partial I^{\alpha}}\right|\overline{\Delta I^{\alpha}}+\left|\frac{\partial\gamma^{\alpha}\left(m_c,I_c,k_{hc},k_{\theta c},U\right)}{\partial k_h{}^{\alpha}}\right|\overline{\Delta k_h^{\alpha}}\\&+\left|\frac{\partial\gamma^{\alpha}\left(m_c,I_c,k_{hc},k_{\theta c},,U\right)}{\partial k_\theta{}^{\alpha}}\right|\overline{\Delta k_\theta^{\alpha}}\end{aligned}, \tag{26}$$

$$\begin{aligned}\underline{\gamma^{\alpha}}\left(m,I,k_h,k_\theta,U\right)&=\gamma^{\alpha}\left(m_c,I_c,k_{hc},k_{\theta c},U\right)+\left|\frac{\partial\gamma^{\alpha}\left(m_c,I_c,k_{hc},k_{\theta c},U\right)}{\partial m^{\alpha}}\right|\underline{\Delta m^{\alpha}}\\&+\left|\frac{\partial\gamma^{\alpha}\left(m_c,I_c,k_{hc},k_{\theta c},U\right)}{\partial I^{\alpha}}\right|\underline{\Delta I^{\alpha}}+\left|\frac{\partial\gamma^{\alpha}\left(m_c,I_c,k_{hc},k_{\theta c},U\right)}{\partial k_h{}^{\alpha}}\right|\underline{\Delta k_h^{\alpha}}\\&+\left|\frac{\partial\gamma^{\alpha}\left(m_c,I_c,k_{hc},k_{\theta c},U\right)}{\partial k_\theta{}^{\alpha}}\right|\underline{\Delta k_\theta^{\alpha}}\end{aligned}. \tag{27}$$

Using equations (26) and (27) at each α-cut, the flutter airspeed membership function can be obtained, and is shown in Figure 13. The flutter boundary range can be seen as a triangular fuzzy mountain shape. For each value of modal damping and at every α-cut, the upper and lower bounds of the flutter speed can be extracted. Values corresponding to $\alpha = 0$ are the largest intervals, and the value corresponding to $\alpha = 1$ is deterministic.

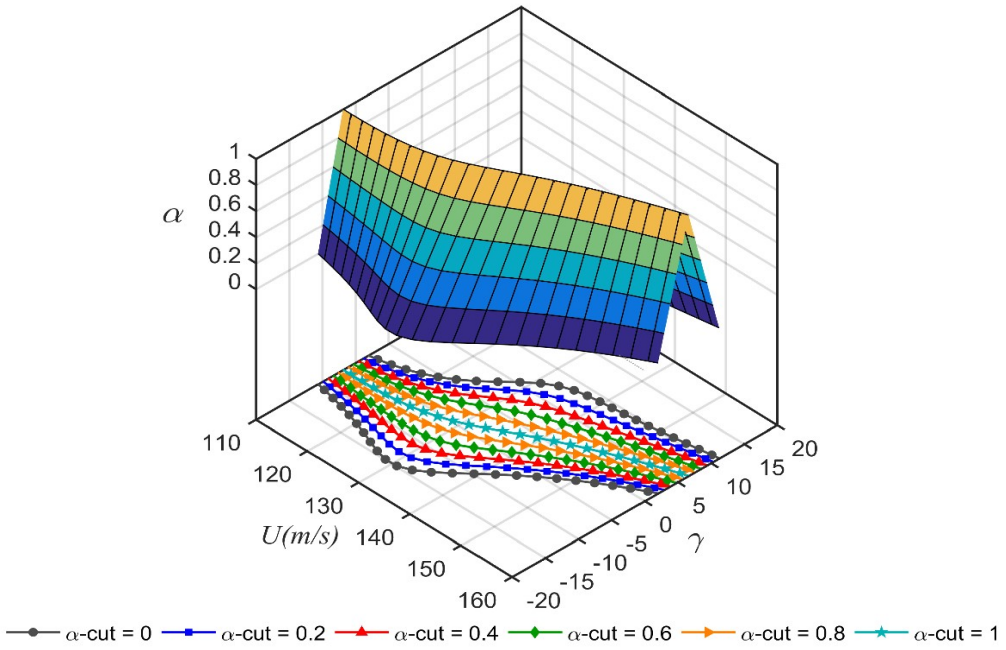

Figure 13. Three-dimensional plot of modal damping versus airspeed for different α-cuts.

In the following, the flutter safety of the wing for six different cases is examined. The 3D interference of air speed and flutter speed is shown in Figure 14. A triangle membership function for airspeed is a reasonable assumption since the airspeed is not a crisp value but varies within intervals. The value which is most possible is the maximum value (α =1) and the value which is least possible is the minimum value (α =0). Furthermore, the triangle membership function is suitable for simplicity to show the concept. In this example the aim is to model airspeed as a fuzzy membership function, not using interval or probabilistic models, to calculate reliability. This method is general, and other arbitrary airspeed membership functions which are more realistic could be used.

In Case 1, it is assumed that the fuzzy air speed is (115,120,125) m/s. This means that the possibility of the air speed for values less than 115 m/s and more than 125 m/s is zero, and the possibility that the air speed is 120 m/s equals one. Based on this assumption the 3D interface between the air speed and the flutter speed is shown in Figure 14(a). Using equation (20) the fuzzy flutter safety can be obtained as

$$S_F = \frac{V_s}{V} = 1 - \frac{V_f}{V} = 1 - \frac{0.41826}{123.5848} = 99.66\%. \tag{28}$$

In Case 2, by keeping the crisp value unchanged, the air speed interval is assumed to be larger. In this case, it is assumed that the fuzzy air speed is (100,120,140) m/s. As shown in Figure 14(b), the failure region interference expands and the flutter safety decreases. The flutter safety value is decreased to 93.91%, in this case.

In Case 3, the air speed intervals are the same as in Case 1, but the crisp value is increased. In this case, it is assumed that the fuzzy air speed is (150, 155,160) m/s, so that the air speed region is larger than the flutter speed in this case. The flutter safety decreases significantly and the flutter reliability reduces to 1.654%. The interference for this case is shown in Figure 14(c). In Case 4, it is assumed that the fuzzy air speed is (105, 110,115) m/s. Figure 14(d) shows that the reliability value increases to 100 due to the lack of interference between the air speed and the flutter speed regions. In Case 5, as can be seen in Figure 14(e), an asymmetric air speed region is considered. It is assumed that the fuzzy wind speed is (100,120,125) m/s. In this case the flutter safety value is 99.87%. Finally, in Case 6, it is assumed that the fuzzy wind speed is (115, 120,140) m/s. Figure 14(f) shows that the difference between the minimum values and the crisp value is less than the difference between the maximum value and the crisp value. In this case, the flutter safety value reduces to 90.23%.

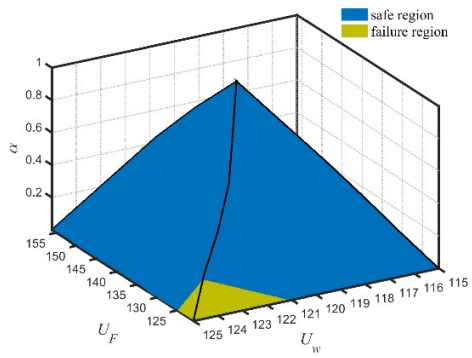

(a)

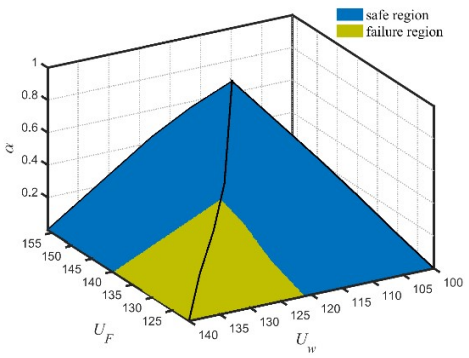

(b)

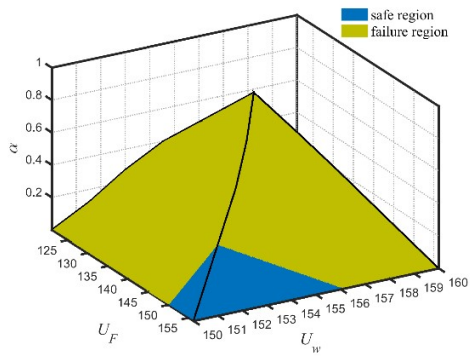

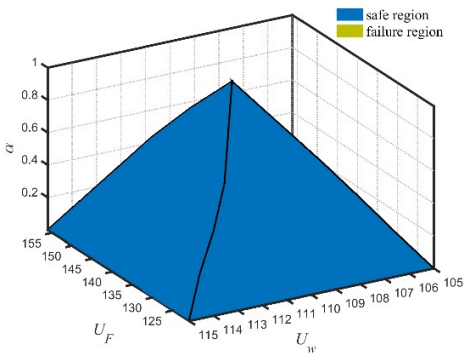

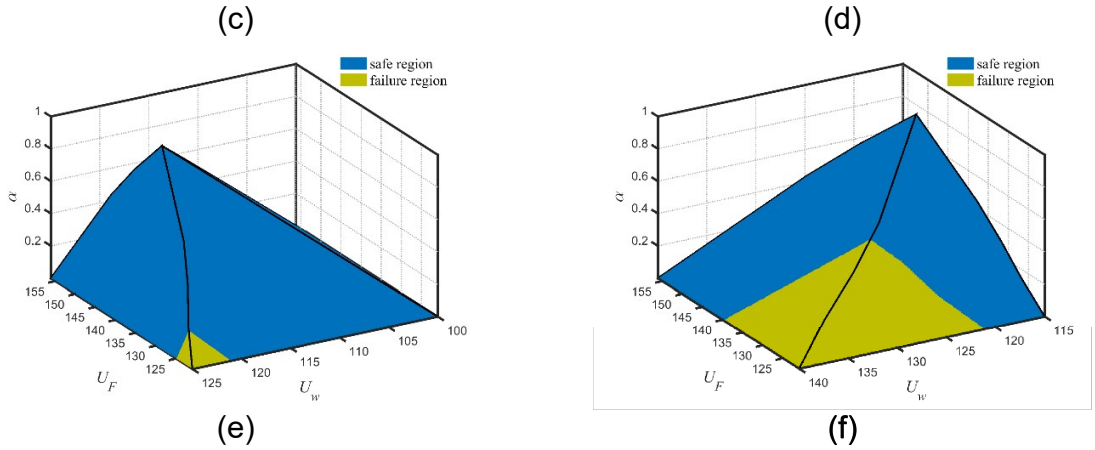

Figure 14. Air speed and flutter speed 3D interference. (a) Case 1, (b) Case 2, (c) Case 3, (d) Case 4, (e) Case 5, (f) Case 6.

Finally, the impact of the number of α-cuts on the accuracy of the reliability is studied. Table 3 and Figure 15 shows the reliability versus the number of α-cuts for the six cases defined earlier. The relative error is defined as

$$Err = \frac{\left|R_e^i - R_e^j\right|}{R_e^j}, \begin{cases} i : \text{number of } \alpha\text{-cut} \\ j : \text{Maximum number of } \alpha\text{-cut} \end{cases} . \tag{29}$$

The results show that, when the number of α-cuts more than 100, the error is almost zero. In this study, the maximum number of α-cuts is set equal to 1000 to guarantee the accuracy of the simulation.

To verify the results the aforementioned method is also compared with Monte Carlo Simulation to verify the integration accuracy. The results are shown in Table 4. The results show that the method has high accuracy relative to the Monte Carlo method with low computational cost.

Table 3
Number of α-cuts and its impact on the accuracy of the flutter reliability

Number of α-Cuts	Reliability											
	Case 1		Case 2		Case 3		Case 4		Case 5		Case 6	
	Reliability	Relative Error	Reliability	Relative Error	Reliability	Relative Error	Reliability	Relative Error	Reliability	Relative Error	Reliability	Relative Error
1	0.9962	0.0010	0.9370	0.0050	0.0124	0.0998	1.0000	0.0000	0.9985	0.0004	0.8992	0.0083
2	0.9956	0.0003	0.9333	0.0010	0.0131	0.0501	1.0000	0.0000	0.9982	0.0001	0.8933	0.0017
3	0.9954	0.0002	0.9329	0.0005	0.0135	0.0239	1.0000	0.0000	0.9982	0.0001	0.8926	0.0009
4	0.9954	0.0001	0.9328	0.0004	0.0138	0.0051	1.0000	0.0000	0.9982	0.0001	0.8924	0.0007
5	0.9954	0.0001	0.9328	0.0004	0.0138	0.0041	1.0000	0.0000	0.9981	0.0001	0.8925	0.0007
6	0.9953	0.0000	0.9325	0.0001	0.0139	0.0035	1.0000	0.0000	0.9981	0.0000	0.8920	0.0001
7	0.9954	0.0001	0.9327	0.0003	0.0138	0.0030	1.0000	0.0000	0.9981	0.0000	0.8923	0.0006
8	0.9953	0.0001	0.9326	0.0002	0.0137	0.0075	1.0000	0.0000	0.9981	0.0000	0.8922	0.0004
9	0.9953	0.0001	0.9326	0.0002	0.0138	0.0042	1.0000	0.0000	0.9981	0.0000	0.8921	0.0003
10	0.9953	0.0001	0.9326	0.0002	0.0139	0.0033	1.0000	0.0000	0.9981	0.0000	0.8922	0.0004
12	0.9952	0.0000	0.9324	0.0000	0.0139	0.0048	1.0000	0.0000	0.9981	0.0000	0.8919	0.0001
14	0.9954	0.0001	0.9327	0.0003	0.0139	0.0067	1.0000	0.0000	0.9981	0.0000	0.8923	0.0005
16	0.9953	0.0000	0.9325	0.0002	0.0138	0.0017	1.0000	0.0000	0.9981	0.0000	0.8921	0.0003
18	0.9953	0.0000	0.9324	0.0000	0.0139	0.0039	1.0000	0.0000	0.9981	0.0000	0.8919	0.0000
20	0.9953	0.0000	0.9326	0.0002	0.0140	0.0103	1.0000	0.0000	0.9981	0.0000	0.8921	0.0003
30	0.9953	0.0000	0.9325	0.0001	0.0139	0.0030	1.0000	0.0000	0.9981	0.0000	0.8920	0.0002
40	0.9953	0.0000	0.9325	0.0002	0.0139	0.0028	1.0000	0.0000	0.9981	0.0000	0.8921	0.0003
50	0.9953	0.0000	0.9324	0.0000	0.0138	0.0049	1.0000	0.0000	0.9981	0.0000	0.8919	0.0001
60	0.9952	0.0000	0.9324	0.0000	0.0139	0.0023	1.0000	0.0000	0.9981	0.0000	0.8919	0.0000
70	0.9953	0.0000	0.9324	0.0000	0.0139	0.0026	1.0000	0.0000	0.9981	0.0000	0.8919	0.0001
80	0.9953	0.0000	0.9325	0.0001	0.0138	0.0002	1.0000	0.0000	0.9981	0.0000	0.8920	0.0002
90	0.9952	0.0000	0.9324	0.0001	0.0138	0.0014	1.0000	0.0000	0.9981	0.0000	0.8919	0.0001
100	0.9952	0.0000	0.9324	0.0000	0.0138	0.0015	1.0000	0.0000	0.9981	0.0000	0.8918	0.0000
200	0.9953	0.0000	0.9324	0.0000	0.0138	0.0003	1.0000	0.0000	0.9981	0.0000	0.8919	0.0000
500	0.9952	0.0000	0.9324	0.0000	0.0138	0.0001	1.0000	0.0000	0.9981	0.0000	0.8918	0.0000
1000	0.9952	0.0000	0.9324	0.0000	0.0138	0.0000	1.0000	0.0000	0.9981	0.0000	0.8918	0.0000

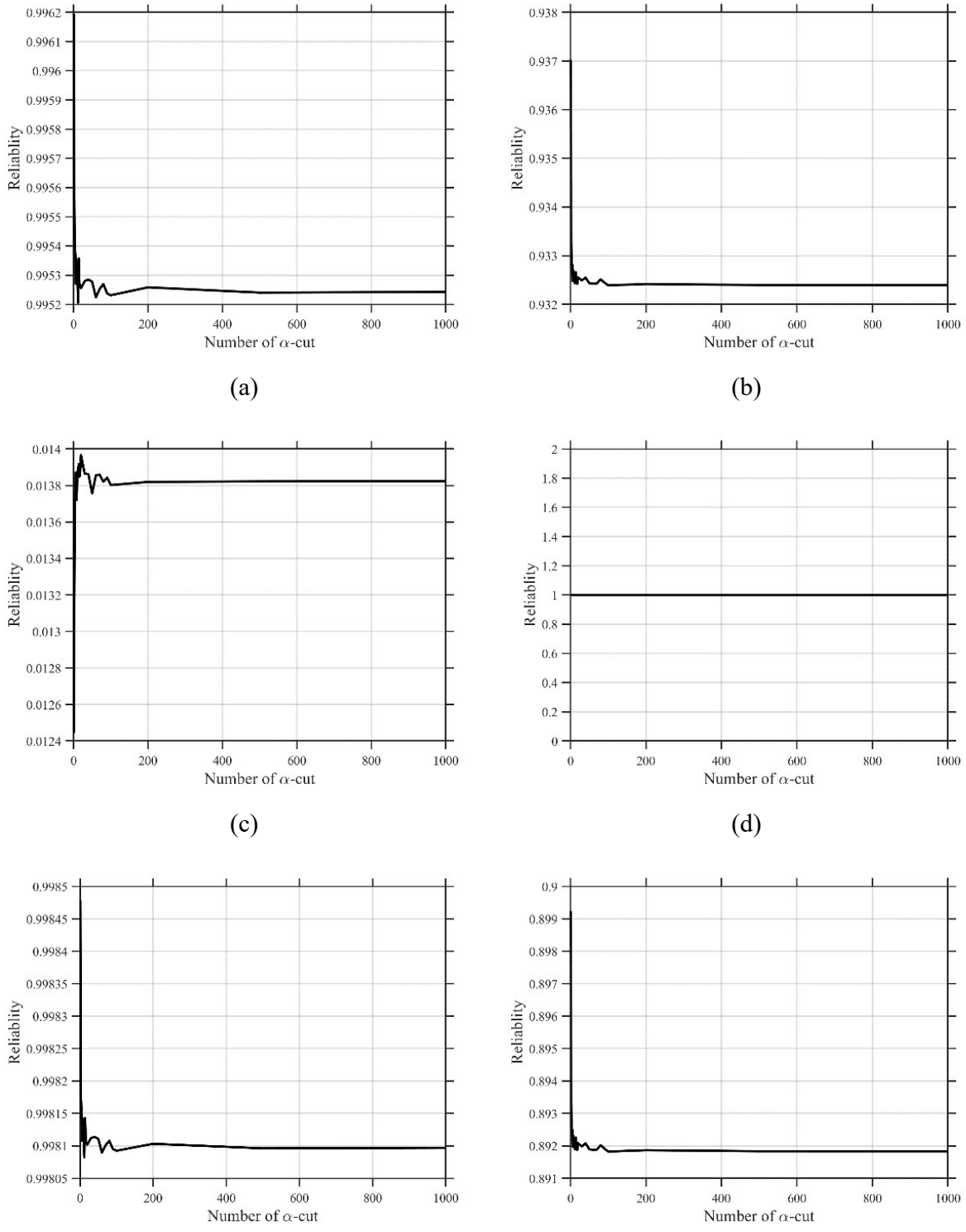

Figure 15. Reliability versus number of α-cuts. (a) Case 1, (b) Case 2, (c) Case 3, (d) Case 4, (e) Case 5, (f) Case 6.

Table 4
The reliability of typical section wing flutter speed with 1000 α-cuts

		Wing Typical Section		
	Method (Number of Simulations)	Fuzzy (2001)	Monte Carlo (1000000)	
	Airspeed Membership Function	Reliability	Reliability	error
Case 1	(115,120,125)	99.52 %	99.82%	0.3%
Case 2	(100,120,140)	93.24 %	95.27%	2.1%
Case 3	(150,155,160)	1.382 %	1.42%	2.6%
Case 4	(105,110,115)	100 %	100%	0%
Case 5	(100,120,125)	99.81 %	99.93%	0.1%
Case 6	(115,120,140)	89.18 %	92.41%	3.4%

5.2. Example 2: Clean Wing

In this example the reliability of a clean wing, which is a famous benchmark model in wing aeroelasticity, is considered. This model is a cantilever beam with bending and torsional deflection as shown in Figure 16.

Suppose that the wing bending and torsional rigidity, wing mass per unit length and moment of inertia per unit length are considered as uncertain fuzzy parameters. The fuzzy triangle membership functions of the uncertain parameters are assumed to be $\overline{m} = (.95m, m, 1.05m)$, $\overline{I_P} = (.95I_P, I_P, 1.05I_P)$, $\overline{EI} = (.95EI, EI, 1.05EI)$ and $\overline{GJ} = (.95GJ, GJ, 1.05GJ)$.

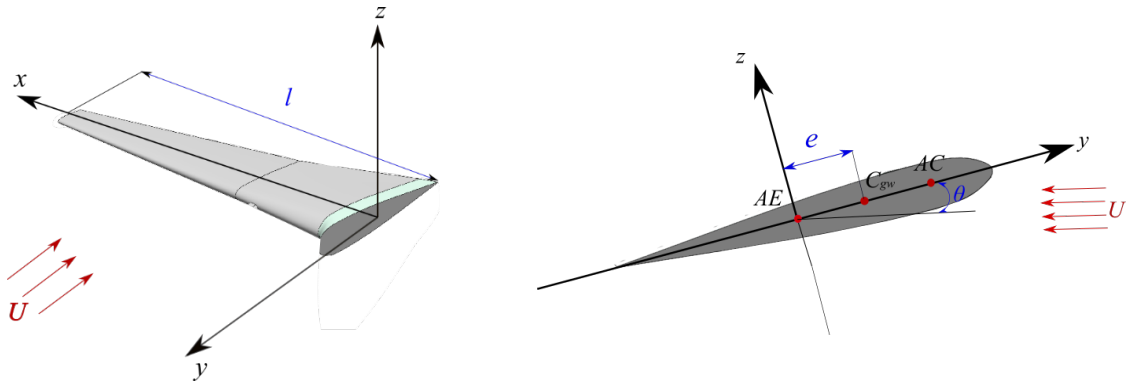

(a) (b)

Figure 16. (a) Schematic of the clean wing, and (b) the typical section wing

Using Hamilton's Principle, the wing equations of motion are obtained as

$$EIw'''' + m\ddot{w} + my_\theta \ddot{\theta} = L \tag{30}$$

$$-GJ\theta'' + I_P \ddot{\theta} + my_\theta \ddot{w} = M \tag{31}$$

where EI and GJ are the bending and torsional rigidity, respectively, m is the wing mass per unit length and I_P is the wing moment of inertia per unit length. Also, L and M are aerodynamic lift and moment, respectively.

The aerodynamic lift and moment based on Peters unsteady aerodynamic theory [39] are used in equations (30) and (31). The aeroelastic governing equations are given by:

$$\begin{aligned}&\left[m_{(x)} + \pi\rho b^2\right]\ddot{w} + \left[m_{(x)}y_\theta + \pi\rho ab^3\right]\ddot{\theta} + U\left[C_{L\theta}\rho b\right]\dot{w} + U\left[-\pi\rho b^2 + C_{L\theta}\rho ab^2 - C_{L\theta}\rho\frac{b^2}{2}\left(\frac{C_{L\theta}}{\pi} - 1\right)\right]\dot{\theta} \\ &+\left[EI\right]w'''' + U\left[C_{L\theta}\rho b\right]\lambda_0(t) - U^2\left[C_{L\theta}\rho b\right]\theta = 0\end{aligned} \tag{32}$$

$$\begin{aligned}&\left[m_{(x)}k_{EA}^2 + \pi\rho b^4\left(\frac{1}{8} + a^2\right)\right]\ddot{\theta} + \left[m_{(x)}y_\theta + \pi\rho ab^3\right]\ddot{w} + U\left[\pi\rho\frac{b^3}{2}\left(\frac{C_{L\theta}}{\pi} - 1\right) - \pi\rho ab^3 + C_{L\theta}\rho ab^3\left(a + \frac{1}{2}\right)\right. \\ &\left.-C_{L\theta}\rho\frac{b^3}{2}\left(\frac{C_{L\theta}}{\pi} - 1\right)\left(a + \frac{1}{2}\right)\right]\dot{\theta} + U\left[C_{L\theta}\rho b^2\left(a + \frac{1}{2}\right)\right]\dot{w} - GJ\theta'' + U\left[C_{L\theta}\rho b^2\left(a + \frac{1}{2}\right)\right]\lambda_0(t) \\ &-U^2\left[C_{L\theta}\rho b^2\left(a + \frac{1}{2}\right)\right]\theta = 0\end{aligned} \tag{33}$$

By discretizing the above equations with the Galerkin method, and solving the final eigenvalue problem, the flutter airspeed and frequency based on the Goland wing parameters are given in Table 2. The results show that this 3D model with finite state unsteady aerodynamic loading is in good agreement with the literature. Furthermore, as expected, the results are more accurate than the 2D equivalent Goland wing typical section model.

By applying the fuzzy interval method described previously, the modal damping for each α-cut is obtained as:

$$\begin{aligned}&\overline{\gamma^\alpha}\left[(EI),(GJ),m,I_P,U\right] = \gamma^\alpha\left[(EI)_c,(GJ)_c,m_c,I_{Pc},U\right] \\ &+\left|\frac{\partial\gamma^\alpha\left[(EI)_c,(GJ)_c,m_c,I_{Pc},U\right]}{\partial(EI)^\alpha}\right|\overline{\Delta(EI)^\alpha} + \left|\frac{\partial\gamma^\alpha\left[(EI)_c,(GJ)_c,m_c,I_{Pc},,U\right]}{\partial(GJ)^\alpha}\right|\overline{\Delta(GJ)^\alpha}, \\ &+\left|\frac{\partial\gamma^\alpha\left[(EI)_c,(GJ)_c,m_c,I_{Pc},U\right]}{\partial m^\alpha}\right|\overline{\Delta m_{(x)}{}^\alpha} + \left|\frac{\partial\gamma^\alpha\left[(EI)_c,(GJ)_c,m_c,I_{Pc},,U\right]}{\partial I_P{}^\alpha}\right|\overline{\Delta I_{P(x)}{}^\alpha}\end{aligned} \tag{34}$$

$$\underline{\gamma^{\alpha}}\left[(EI),(GJ),m,I_P,U\right]=\gamma^{\alpha}\left[(EI)_c,(GJ)_c,m_c,I_{Pc},U\right]$$
$$+\left|\frac{\partial\gamma^{\alpha}\left[(EI)_c,(GJ)_c,m_c,I_{Pc},U\right]}{\partial(EI)^{\alpha}}\right|\underline{\Delta(EI)^{\alpha}}+\left|\frac{\partial\gamma^{\alpha}\left[(EI)_c,(GJ)_c,m_c,I_{Pc},,U\right]}{\partial(GJ)^{\alpha}}\right|\underline{\Delta(GJ)^{\alpha}}\quad .\qquad (35)$$
$$+\left|\frac{\partial\gamma^{\alpha}\left[(EI)_c,(GJ)_c,m_c,I_{Pc},U\right]}{\partial m^{\alpha}}\right|\underline{\Delta m^{\alpha}}+\left|\frac{\partial\gamma^{\alpha}\left[(EI)_c,(GJ)_c,m_c,I_{Pc},,U\right]}{\partial I_P{}^{\alpha}}\right|\underline{\Delta I_P{}^{\alpha}}$$

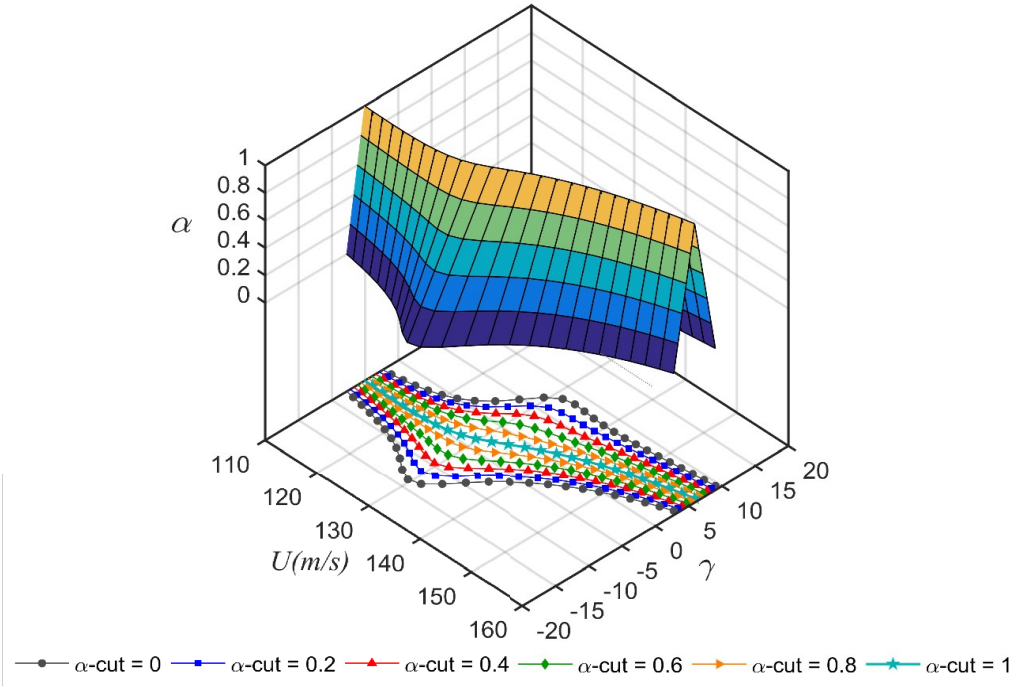

Figure 17. Three-dimensional plot of modal damping versus airspeed for different α-cuts.

To obtain the flutter fuzzy membership function the dominant mode which can cause flutter is considered. In this example the first bending mode is dominant and the other modes are stable.

Using equations (31) and (32) at each α-cut, the flutter airspeed membership function can be obtained, as shown in Figure 17. The flutter boundary range can be seen as a triangle fuzzy mountain shape. Indeed, for each value of the modal damping and at every α-cut, the upper and lower bounds of the flutter speed can be extracted from this figure.

The reliability analysis for all cases which were studied in example 1 is also carried out for this example and the results are given in Table 5. As expected, the results are very similar to the results of the previous example because of the similar properties of the two models. Obviously, since a

more accurate aeroelastic model was used in this example, the results are more accurate than the typical section model results.

Table 5
The fuzzy reliability of wing flutter speed

	Airspeed Membership Function	Typical Section	Clean Wing
		Fuzzy Reliability	Fuzzy Reliability
Case 1	(115,120,125)	99.52 %	99.75 %
Case 2	(100,120,140)	93.24 %	92.69 %
Case 3	(150,155,160)	1.382 %	1.28e-3 %
Case 4	(105,110,115)	100 %	100 %
Case 5	(100,120,125)	99.81 %	99.90 %
Case 6	(115,120,140)	89.18 %	88.30 %

6.0 CONCLUSION

In this paper, a new method for the flutter speed reliability analysis of aircraft wings using a fuzzy interval approach is investigated. Uncertain parameters are modeled as fuzzy membership functions and propagated through the wing aeroelastic model. The flutter region at each α-cut is obtained through the P method. By combining the flutter intervals at each α-cut the fuzzy flutter speed membership function is obtained. The interference between the fuzzy flutter area and the air speed area forms a pyramid. The reliability or flutter safety is then obtained from this interference volume.

The prominent advantage of this method is that only membership functions of uncertain parameters are required and the other statistical characteristics or the probabilistic distribution densities are not needed for the reliability analysis. In order to illustrate the feasibility of this fuzzy reliability method, a typical section 2D wing model and a clean wing 3D model were used. For both examples, the reliability analysis is performed for six wind speed conditions and the flutter reliability was determined for each condition. The results show that this approach is a suitable method to predict wing flutter safety.

References

1. ABBAS, T., MORGENTHAL, G. Framework for sensitivity and uncertainty quantification in the flutter assessment of bridges. *Probabilistic Engineering Mechanics*. 2016, **43**, pp 91-105.

2. AFONSO, F., VALE, J., OLIVEIRA, É., LAU, F., SULEMAN, A. Non-linear aeroelastic response of high aspect-ratio wings in the frequency domain. *The Aeronautical Journal*. 2017, **121**, (1240), pp 858-76.
3. AJAJ, R. M., FRISWELL, M. I., DETTMER, W. G., ALLEGRI, G., ISIKVEREN, A. T. Dynamic modelling and actuation of the adaptive torsion wing. *Journal of Intelligent Material Systems and Structures*. 2013, **24**, (16), pp 2045-57.
4. BADCOCK, K. J., TIMME, S., MARQUES, S., et al. Transonic aeroelastic simulation for instability searches and uncertainty analysis. *Progress in Aerospace Sciences*. 2011, **47**, (5), pp 392-423.
5. BIJL, H., LUCOR, D., MISHRA, S., SCHWAB, C. *Uncertainty Quantification in Computational Fluid Dynamics*: Springer Science & Business Media, 2013.
6. BORELLO, F., CESTINO, E., FRULLA, G. Structural uncertainty effect on classical wing flutter characteristics. *Journal of Aerospace Engineering*. 2010, **23**, (4), pp 327-38.
7. BOULKAIBET, I., MARWALA, T., FRISWELL, M. I., KHODAPARAST, H. H., ADHIKARI, S. Fuzzy finite element model updating using metaheuristic optimization algorithms. *Special Topics in Structural Dynamics, Volume 6*: Springer, 2017, p. 91-101.
8. CHIANG, W.-l., DONG, W.-M., WONG, F. S. Dynamic response of structures with uncertain parameters: A comparative study of probabilistic and fuzzy sets models. *Probabilistic Engineering Mechanics*. 1987, **2**, (2), pp 82-91.
9. De GERSEM, H., MOENS, D., DESMET, W., VANDEPITTE, D. Interval and fuzzy dynamic analysis of finite element models with superelements. *Computers & Structures*. 2007, **85**, (5), pp 304-19.
10. Di SCIUVA, M., LOMARIO, D. A comparison between Monte Carlo and FORMs in calculating the reliability of a composite structure. *Composite Structures*. 2003, **59**, (1), pp 155-62.
11. DOWELL, E. H. *A Modern Course in Aeroelasticity*: Springer, 2014.
12. FAZELZADEH, S. A., MAZIDI, A., KALANTARI, H. Bending-torsional flutter of wings with an attached mass subjected to a follower force. *Journal of Sound and Vibration*. 2009, **323**, (1), pp 148-62.
13. FAZELZADEH, S. A., SADAT-HOSEINI, H. Nonlinear flight dynamics of a flexible aircraft subjected to aeroelastic and gust loads. *Journal of Aerospace Engineering*. 2012, **25**, (1), pp 51-63.
14. FAZELZADEH, S. A., RASTI, A., SADAT-HOSEINI, H. Optimal flutter suppression of nonlinear typical wing section using time-domain finite elements method. *Journal of Aerospace Engineering*. 2014, **27**, (5), pp.
15. FAZELZADEH, S. A., AZADI, M., AZADI, E. Suppression of nonlinear aeroelastic vibration of a wing/store under gust effects using an adaptive-robust controller. *Journal of Vibration and Control*. 2017, **23**, (7), pp 1206-17.
16. FAZELZADEH, S. A., GHASEMI, A. H., MAZIDI, A. Aeroelastic analysis of unrestrained aircraft wing with external stores under roll maneuver. *International Journal of Acoustics and Vibration*. 2016, **21**, (3), pp 327-33.
17. FRANGOPOL, D. M., MAUTE, K. Life-cycle reliability-based optimization of civil and aerospace structures. *Computers & Structures*. 2003, **81**, (7), pp 397-410.
18. FRISWELL, M. I., MOTTERSHEAD, J. E. *Finite element model updating in structural dynamics*: Springer Science & Business Media, 1995.
19. GOLAND, M. The flutter of a uniform cantilever wing. *Journal of Applied Mechanics-Transactions of the ASME*. 1945, **12**, (4), pp A197-A208.
20. HADDAD KHODAPARAST, H., GOVERS, Y., DAYYANI, I., et al. Fuzzy finite element model updating of the DLR AIRMOD test structure. A*pplied Mathematical Modelling*. 2017, **52**, pp 512-526
21. HODGES, D. H., PIERCE, G. A. *Introduction to Structural Dynamics and Aeroelasticity*: Cambridge University Press, 2011.
22. HUAN, Z., YUAN, G., CHAO, W. Effective Robust Design of High Lift NLF Airfoil under Multi-Parameter Uncertainty. *Aerospace Science and Technology*. 2017, (pp.
23. KHODAPARAST, H. H., MOTTERSHEAD, J. E., FRISWELL, M. I. Perturbation methods for the estimation of parameter variability in stochastic model updating. *Mechanical Systems and Signal Processing*. 2008, **22**, (8), pp 1751-73.
24. KHODAPARAST, H. H., MOTTERSHEAD, J. E., BADCOCK, K. J. Propagation of structural uncertainty to linear aeroelastic stability. *Computers & Structures*. 2010, **88**, (3), pp 223-36.
25. LOKATT, M. Aeroelastic flutter analysis considering modeling uncertainties. *Journal of Fluids and Structures*. 2017, **74**, (pp 247-62.
26. MANNINI, C., BARTOLI, G. Aerodynamic uncertainty propagation in bridge flutter analysis. *Structural Safety*. 2015, **52**, (pp 29-39.
27. MANSON, G. Sharper eigenproblem estimates for uncertain multi degree-of-freedom systems. *Proceedings of IMAC-XXI, Kissimmee, Florida, USA*. 2003, (pp.
28. MARES, C., MOTTERSHEAD, J. E., FRISWELL, M. I. Stochastic model updating: part 1—theory and simulated example. *Mechanical Systems and Signal Processing*. 2006, **20**, (7), pp 1674-95.
29. MASSA, F., LALLEMAND, B., TISON, T., LEVEL, P. Fuzzy eigensolutions of mechanical structures. *Engineering Computations*. 2004, **21**, (1), pp 66-77.
30. MASSA, F., MOURIER-RUFFIN, K., LALLEMAND, B., TISON, T. Structural analysis by interval approach. *European Journal of Computational Mechanics/Revue Européenne de Mécanique Numérique*. 2008, **17**, (5-7), pp 869-80.
31. MAZIDI, A., KALANTARI, H., FAZELZADEH, S. Aeroelastic response of an aircraft wing with mounted engine subjected to time-dependent thrust. *Journal of Fluids and Structures*. 2013, **39**, pp 292-305.
32. MOENS, D., VANDEPITTE, D. A survey of non-probabilistic uncertainty treatment in finite element analysis. *Computer Methods in Applied Mechanics and Engineering*. 2005, **194**, (12), pp 1527-55.

33. MOTTERSHEAD, J. E., FRISWELL, M. I., NG, G. H. T., BRANDON, J. A. Geometric parameters for finite element model updating of joints and constraints. *Mechanical Systems and Signal Processing*. 1996, **10**, (2), pp 171-82.
34. MUHANNA, R. L., MULLEN, R. L. Uncertainty in mechanics problems—Interval–based approach. *Journal of Engineering Mechanics*. 2001, **127**, (6), pp 557-66.
35. MUHANNA, R. L., ZHANG, H., MULLEN, R. L. Interval finite elements as a basis for generalized models of uncertainty in engineering mechanics. *Reliable Computing*. 2007, **13**, (2), pp 173-94.
36. NGUYEN, N. Integrated flight dynamic modeling of flexible aircraft with inertial force-propulsion-aeroelastic coupling. *46th AIAA Aerospace Sciences Meeting and Exhibit*2008, p. 194.
37. NGUYEN, N., TUZCU, I. Flight dynamics of flexible aircraft with aeroelastic and inertial force interactions. *AIAA Atmospheric Flight Mechanics Conference*2009, p. 6045.
38. OH, D., LIBRESCU, L. Free vibration and reliability of composite cantilevers featuring uncertain properties. *Reliability Engineering & System Safety*. 1997, **56**, (3), pp 265-72.
39. PETERS, D. A., KARUNAMOORTHY, S., CAO, W.-M. Finite state induced flow models part I: Two-dimensional thin airfoil. *Journal of Aircraft*. 1995, **32**, (2), pp 313-22.
40. QIU, Z. Comparison of static response of structures using convex models and interval analysis method. *International Journal for Numerical Methods in Engineering*. 2003, **56**, (12), pp 1735-53.
41. QIU, Z., WANG, X. Comparison of dynamic response of structures with uncertain-but-bounded parameters using non-probabilistic interval analysis method and probabilistic approach. *International Journal of Solids and Structures*. 2003, **40**, (20), pp 5423-39.
42. QIU, Z. Convex models and interval analysis method to predict the effect of uncertain-but-bounded parameters on the buckling of composite structures. *Computer Methods in Applied Mechanics and Engineering*. 2005, **194**, (18), pp 2175-89.
43. RAO, S. S., BERKE, L. Analysis of uncertain structural systems using interval analysis. *AIAA journal*. 1997, **35**, (4), pp 727-35.
44. REZAEI, M., FAZELZADEH, S., MAZIDI, A., KHODAPARAST, H. H. Fuzzy uncertainty analysis in the flutter boundary of an aircraft wing subjected to a thrust force. *Proceedings of the Institution of Mechanical Engineers, Part G: Journal of Aerospace Engineering*. 2018, (pp 0954410018773898.
45. SADAT-HOSEINI, H., FAZELZADEH, S., RASTI, A., MARZOCCA, P. Final approach and flare control of a flexible aircraft in crosswind landings. *Journal of Guidance, Control, and Dynamics*. 2013, **36**, (4), pp 946-57.
46. SARKAR, S., WITTEVEEN, J., LOEVEN, A., BIJL, H. Effect of uncertainty on the bifurcation behavior of pitching airfoil stall flutter. *Journal of Fluids and Structures*. 2009, **25**, (2), pp 304-20.
47. SOFI, A., MUSCOLINO, G., ELISHAKOFF, I. Natural frequencies of structures with interval parameters. *Journal of Sound and Vibration*. 2015, **347**, (pp 79-95.
48. STARCZEWSKI, J. T. *Advanced concepts in fuzzy logic and systems with membership uncertainty*: Springer, 2012.
49. SULEMAN, A., AFONSO, F., VALE, J., OLIVEIRA, É., LAU, F. Non-linear aeroelastic analysis in the time domain of high-aspect-ratio wings: Effect of chord and taper-ratio variation. *The Aeronautical Journal*. 2017, **121**, (1235), pp 21-53.
50. TANG, D., DOWELL, E. H. Flutter/LCO suppression for high-aspect ratio wings. *The Aeronautical Journal*. 2009, **113**, (1144), pp 409-16.
51. TARTARUGA, I., COOPER, J. E., GEORGIOU, G., KHODAPARAST, H. Flutter Uncertainty Quantification for the S4T Model. *55th AIAA Aerospace Sciences Meeting*2017, p. 1653.
52. WANG, L., XIONG, C., HU, J., WANG, X., QIU, Z. Sequential multidisciplinary design optimization and reliability analysis under interval uncertainty. *Aerospace Science and Technology*. 2018, **80**, pp 508-19.
53. WANG, L., XIONG, C., WANG, X., XU, M., LI, Y. A dimension-wise method and its improvement for multidisciplinary interval uncertainty analysis. *Applied Mathematical Modelling*. 2018, **59**, pp 680-95.
54. WANG, L., XIONG, C., YANG, Y. A novel methodology of reliability-based multidisciplinary design optimization under hybrid interval and fuzzy uncertainties. *Computer Methods in Applied Mechanics and Engineering*. 2018, **337**, (pp 439-57.
55. WANG, X., QIU, Z. Nonprobabilistic interval reliability analysis of wing flutter. *AIAA Journal*. 2009, **47**, (3), pp 743-8.
56. WRIGHT, J. R., COOPER, J. E. *Introduction to aircraft aeroelasticity and loads*: John Wiley & Sons, 2008.
57. WU, J., LUO, Z., ZHANG, N. Interval uncertain optimization of structures using Chebyshev meta-models. *Proceedings: the 10th World Congress on Structural and Multidisciplinary Optimization (WCSMO10)*2013.
58. WU, J., ZHANG, Y., CHEN, L., LUO, Z. A Chebyshev interval method for nonlinear dynamic systems under uncertainty. *Applied Mathematical Modelling*. 2013, **37**, (6), pp 4578-91.
59. WANG, X. QIU, Z. Interval finite element analysis of wing flutter. *Chinese Journal of Aeronautics*. 2008, **21**, (2), pp 134-40.
60. YANG, Y., CAI, Z., LIU, Y. Interval analysis of dynamic response of structures using Laplace transform. *Probabilistic Engineering Mechanics*. 2012, **29**, (pp 32-9.
61. YUN, H., HAN, J. Robust flutter analysis of a nonlinear aeroelastic system with parametric uncertainties. *Aerospace Science and Technology*. 2009, **13**, (2-3), pp 139-49.

Figure 1. Triangle fuzzy membership function.

Click here to access/download;Figure;figure1.tif

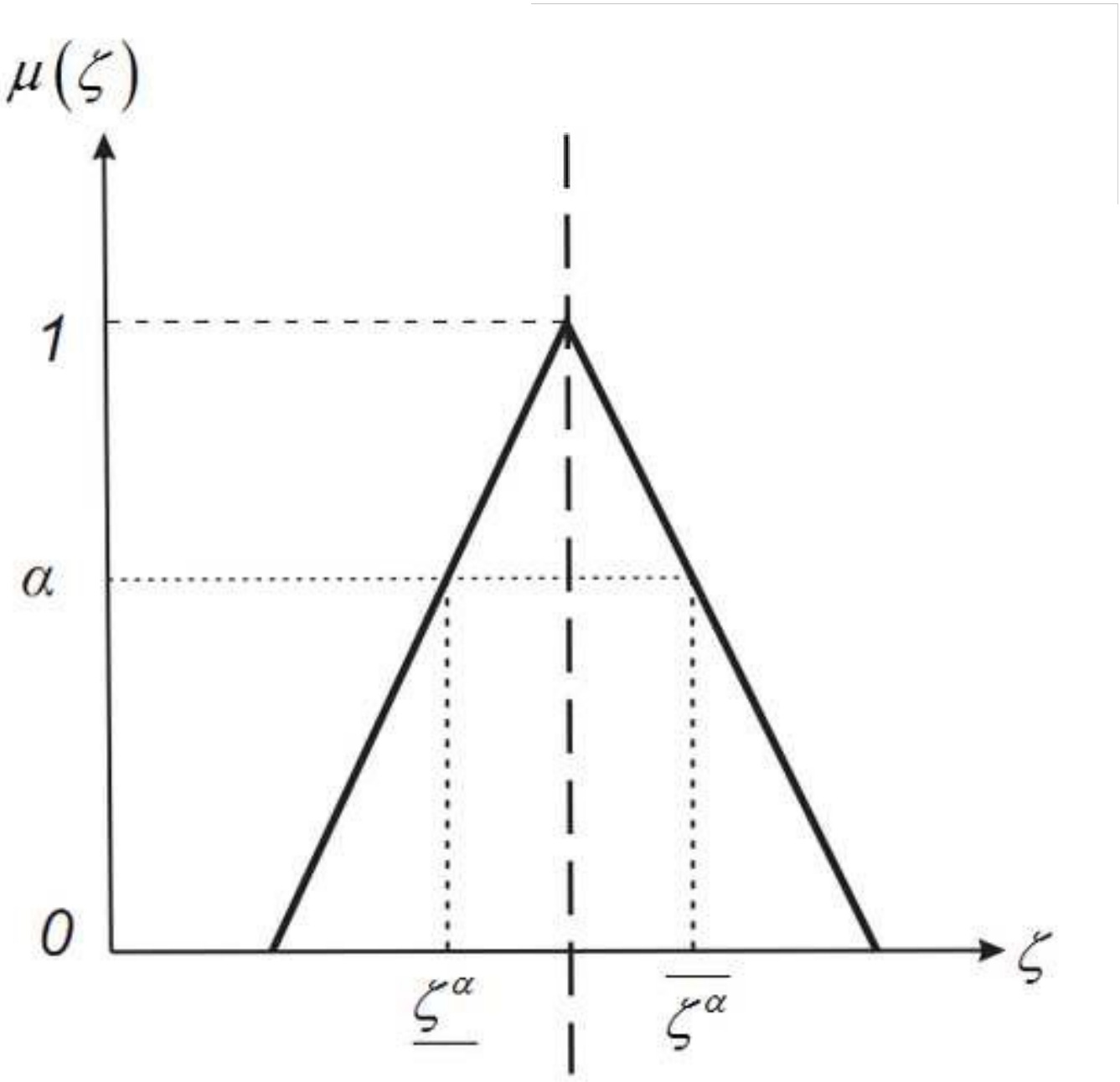

Figure 2. An example flutter speed membership function.

Click here to access/download;Figure;figure2.tif

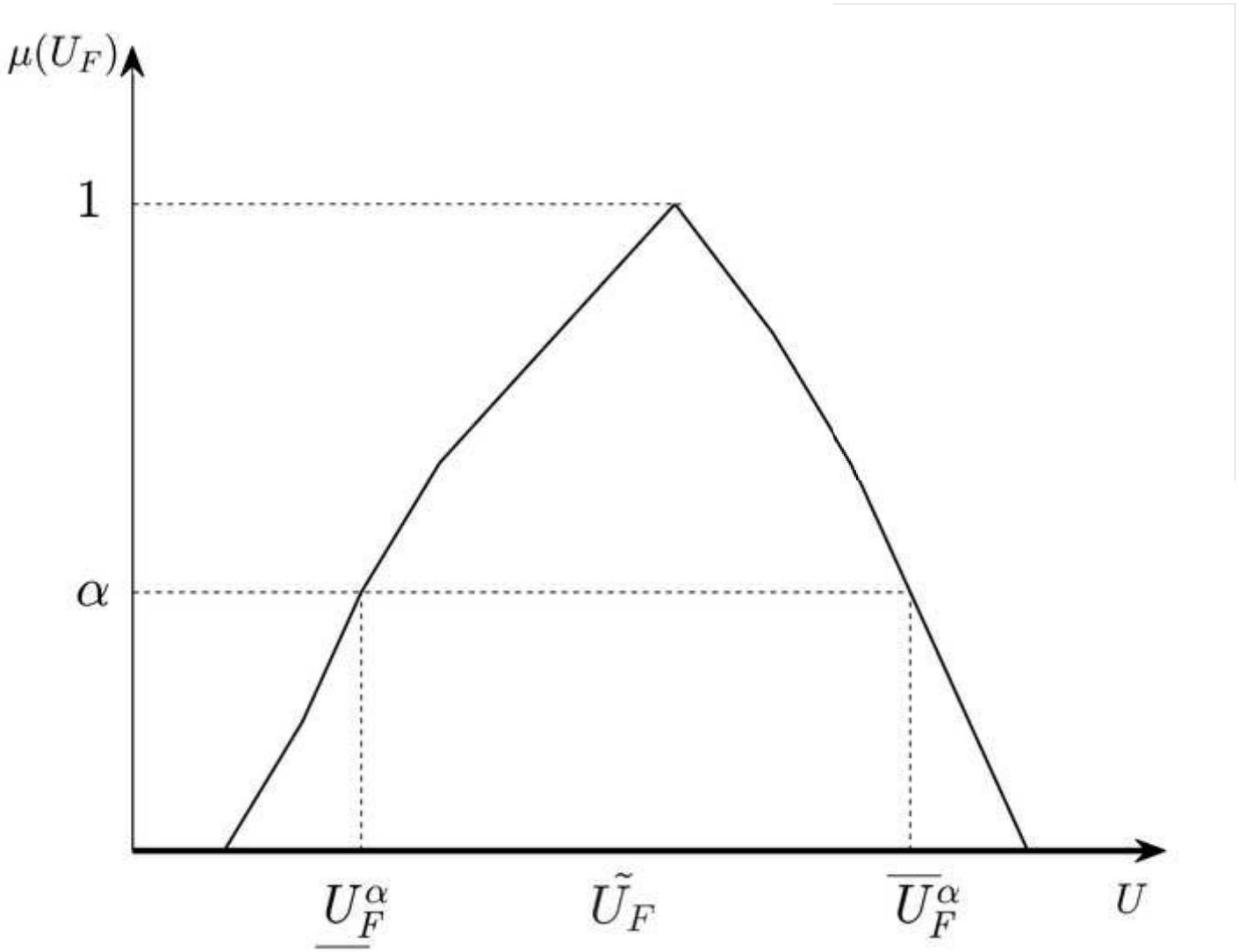

Figure 3. Flutter speed and wind speed 2-D fuzzy interference.

Click here to access/download;Figure;figure3.tif

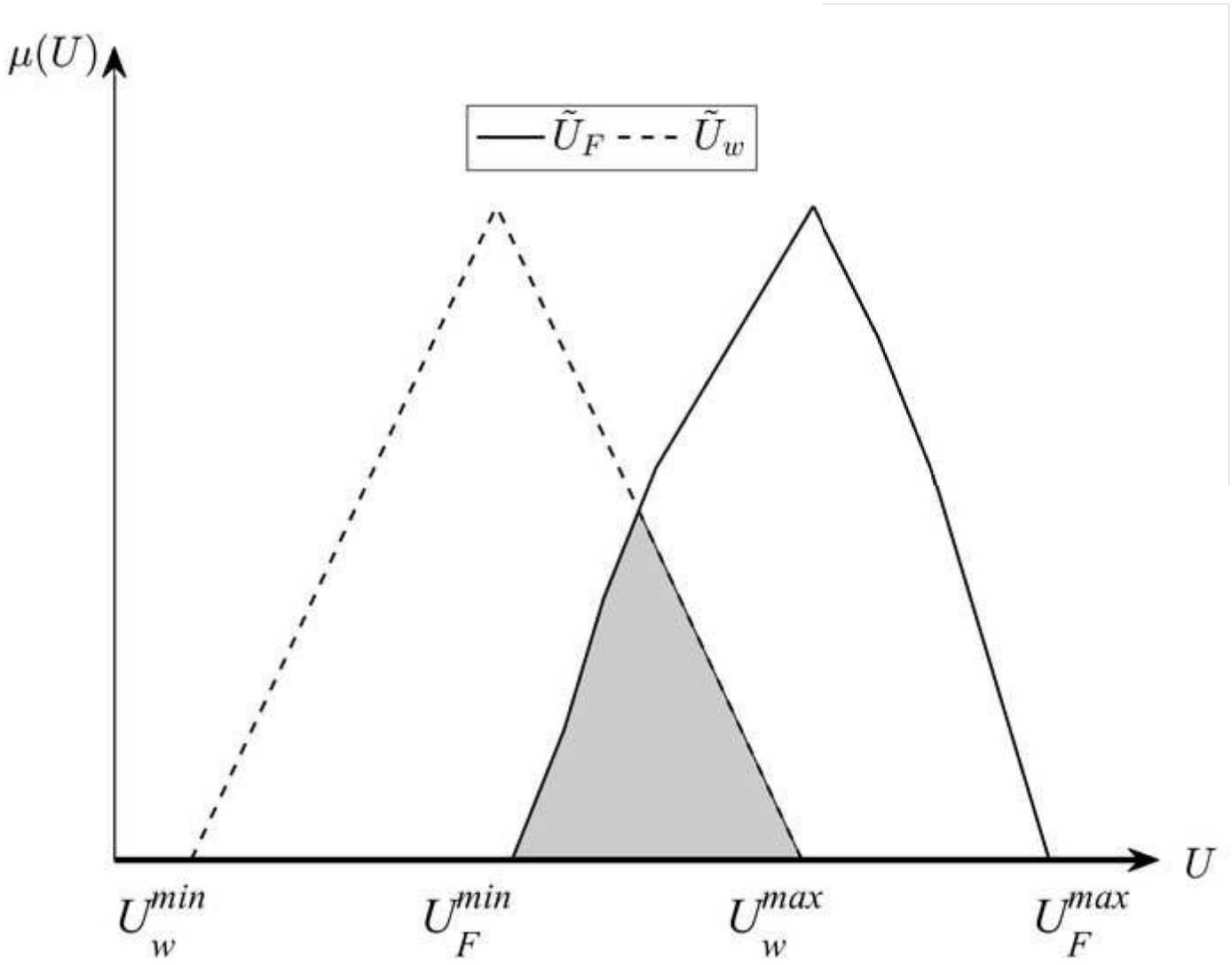

Figure 4. Space of variables under interference occurrence.

Click here to access/download;Figure;Figure4.tif

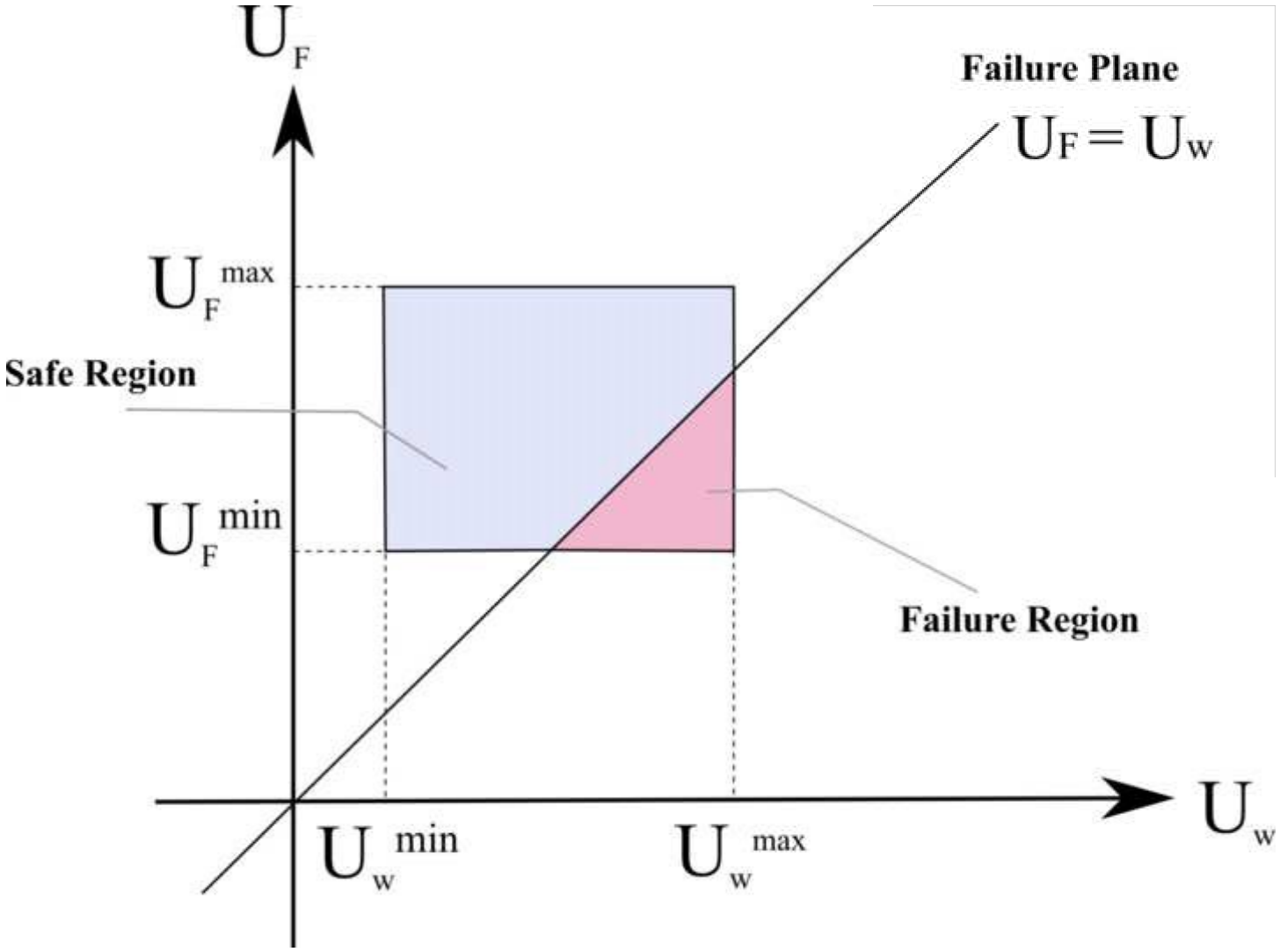

Figure 5. The pyramid of variables in the case of triangular membership functions.

Click here to access/download;Figure;figure5.tif

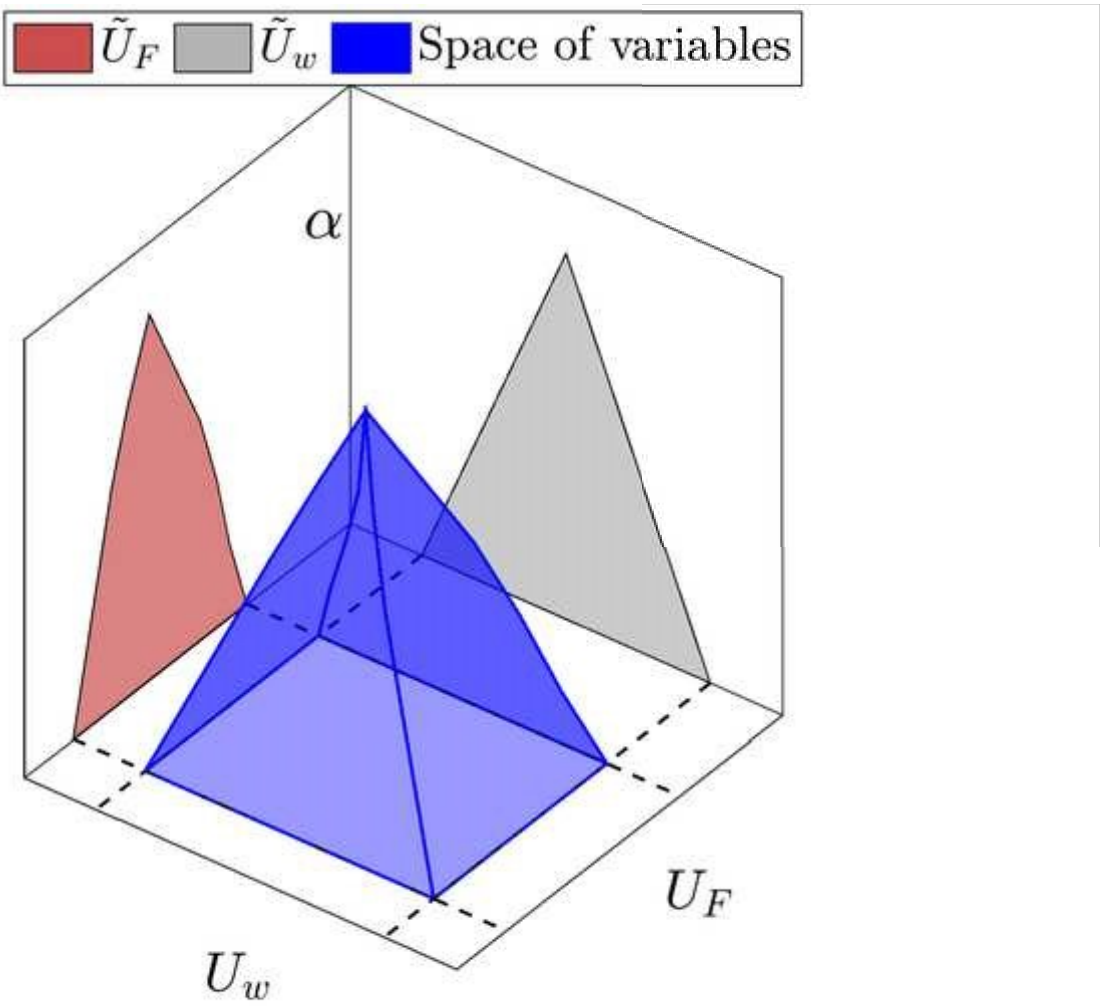

Figure 6. Safe region and failure region.

Click here to access/download;Figure;figure6.tif

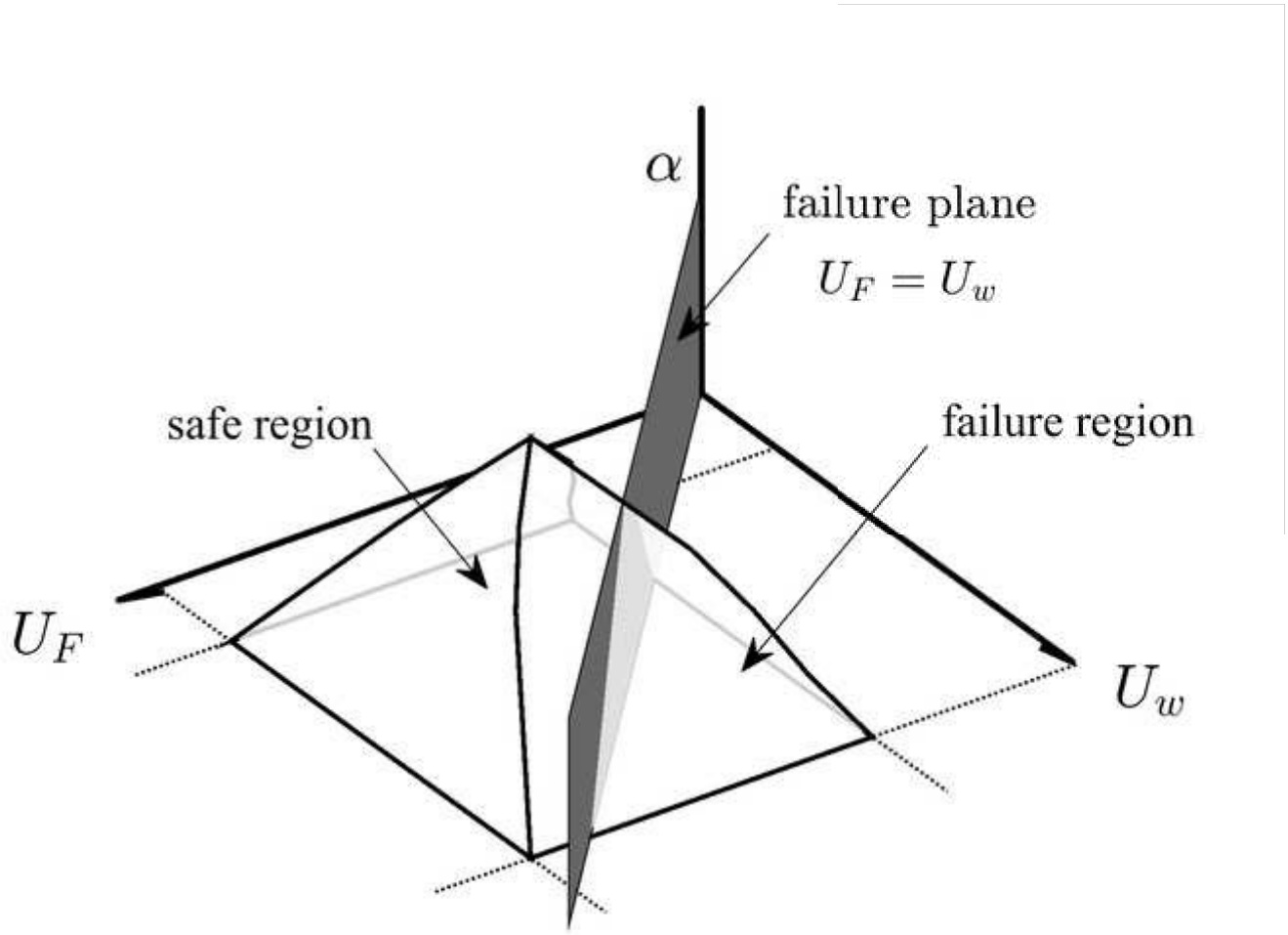

Figure 7. Numerical integration evaluation to obtain the volume of the possible space.

Click here to access/download;Figure;figure7.tif

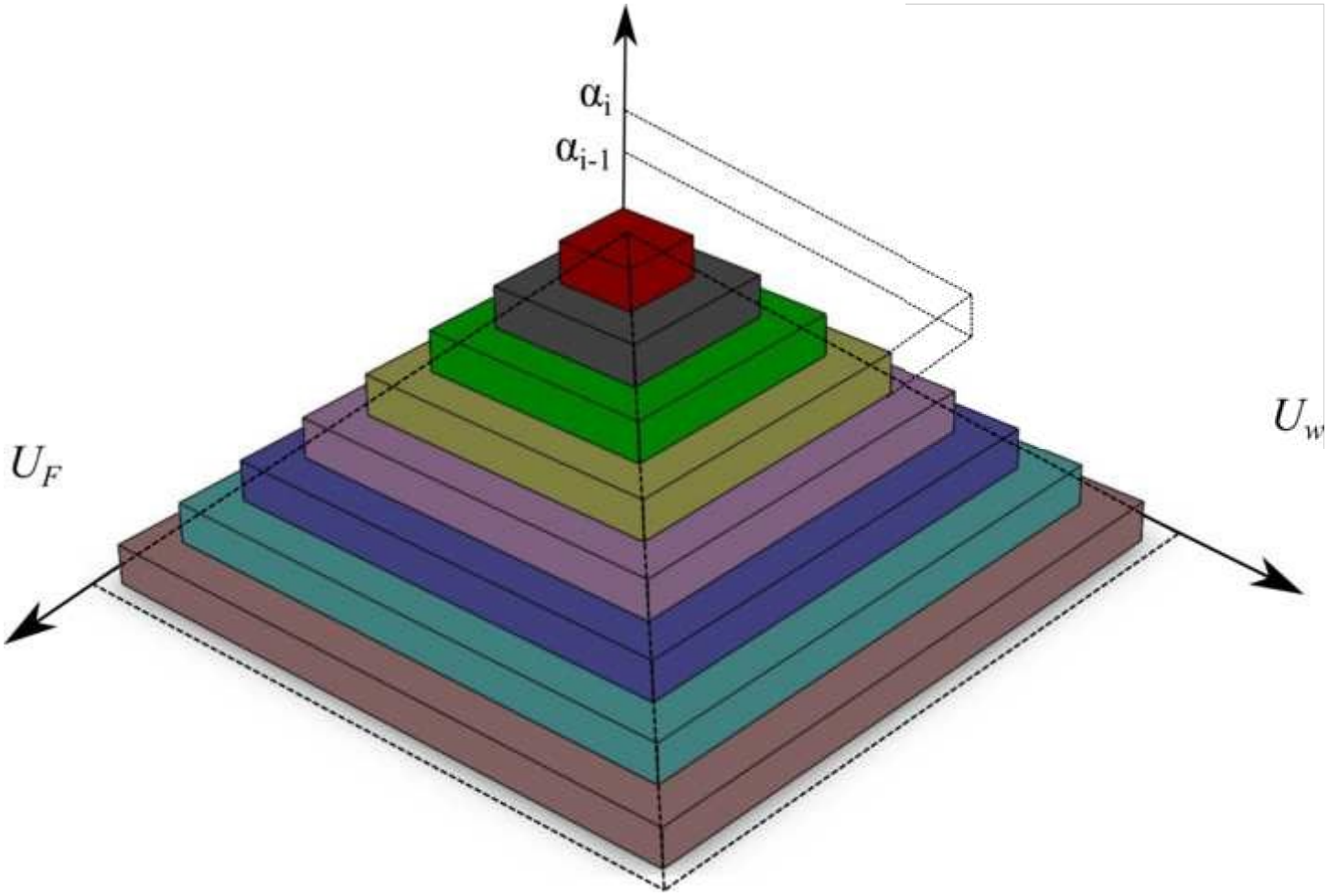

Figure 8. A case in which all parts of the interference volume are in the safe region.

Click here to access/download;Figure;figure8.tif

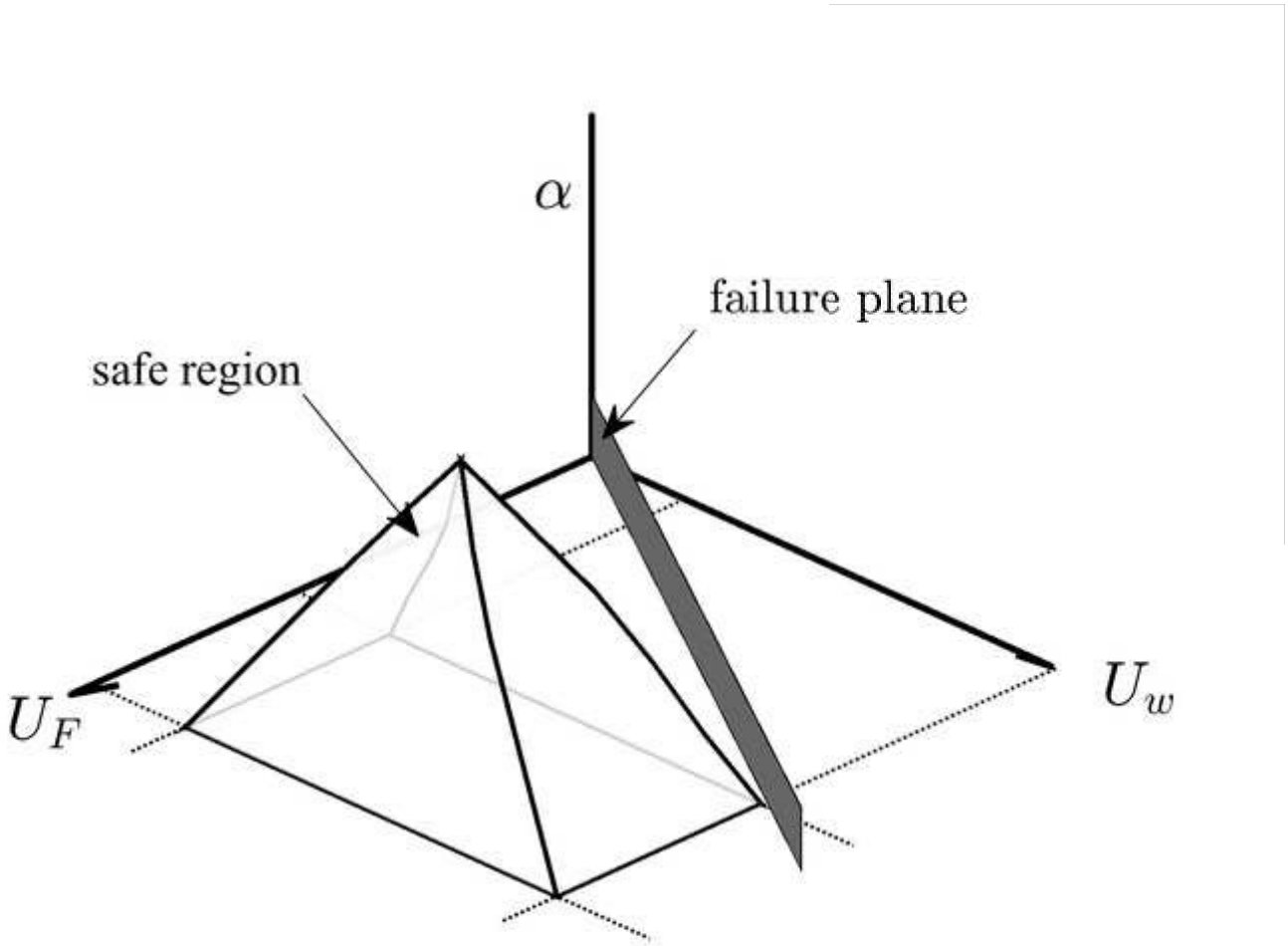

Figure 9. A case in which all parts of the interference volume are in the failure region.

Click here to access/download;Figure;figure9.tif

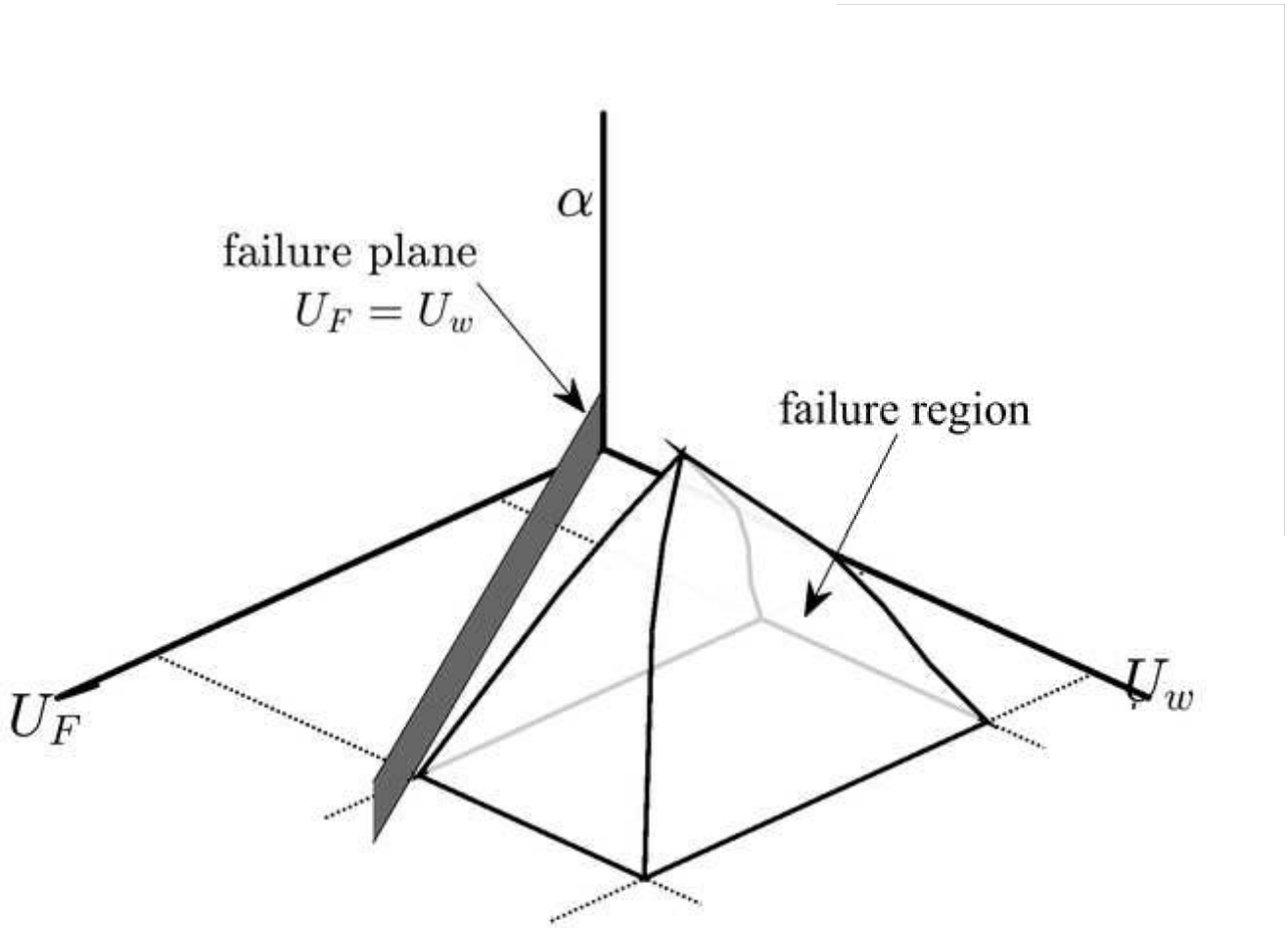

Figure 10. Fuzzy method flowchart

Click here to access/download;Figure;figure10.tif

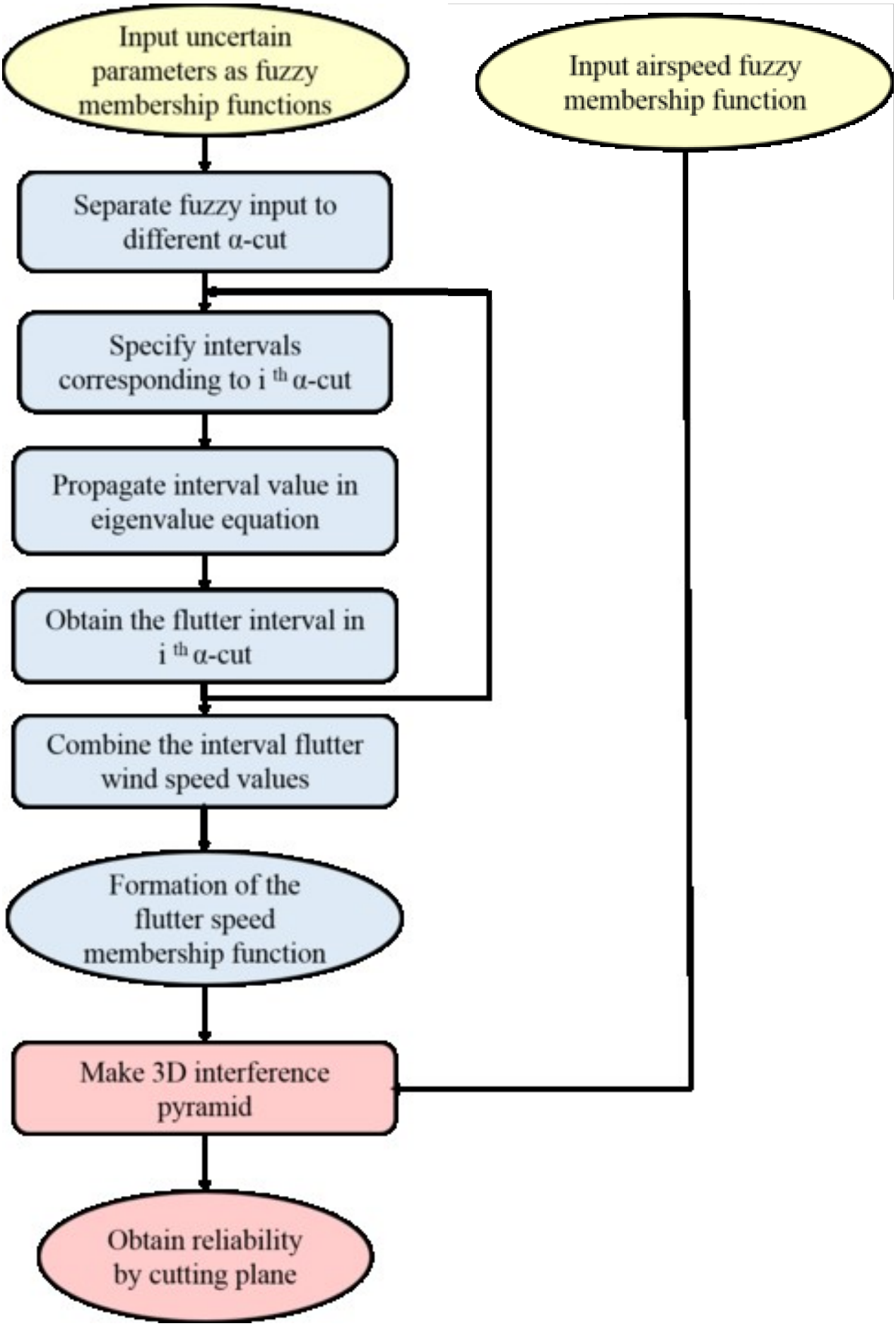

Figure 11. A typical section wing model.

Click here to access/download;Figure;figure11.tif

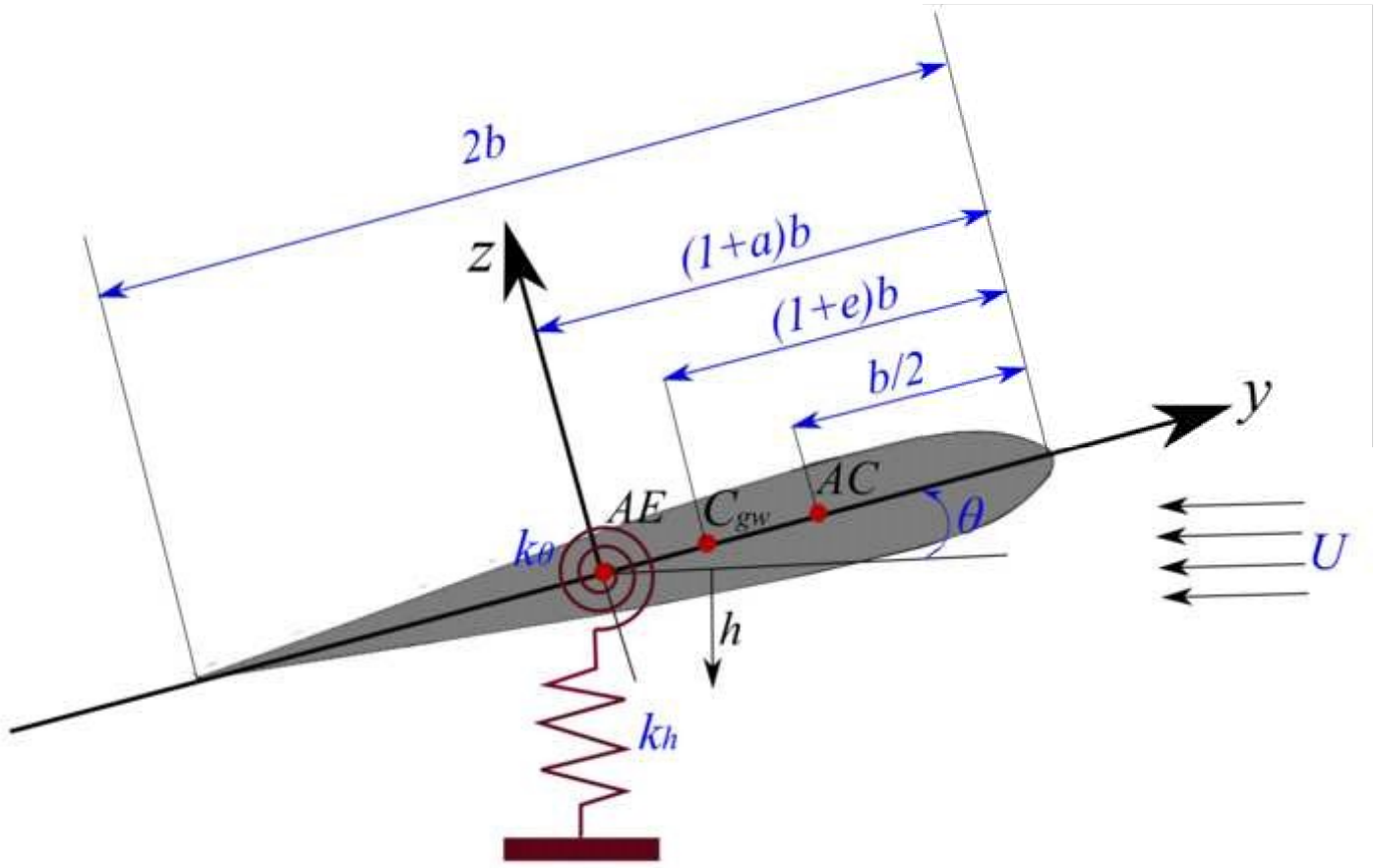

Figure 12. Modal damping versus dimensionless airspeed for a = -0.2, e = 0.1, μ = 20, r2 = 0.24 and σ = 0.4.

Click here to access/download;Figure;Figure 12.jpg

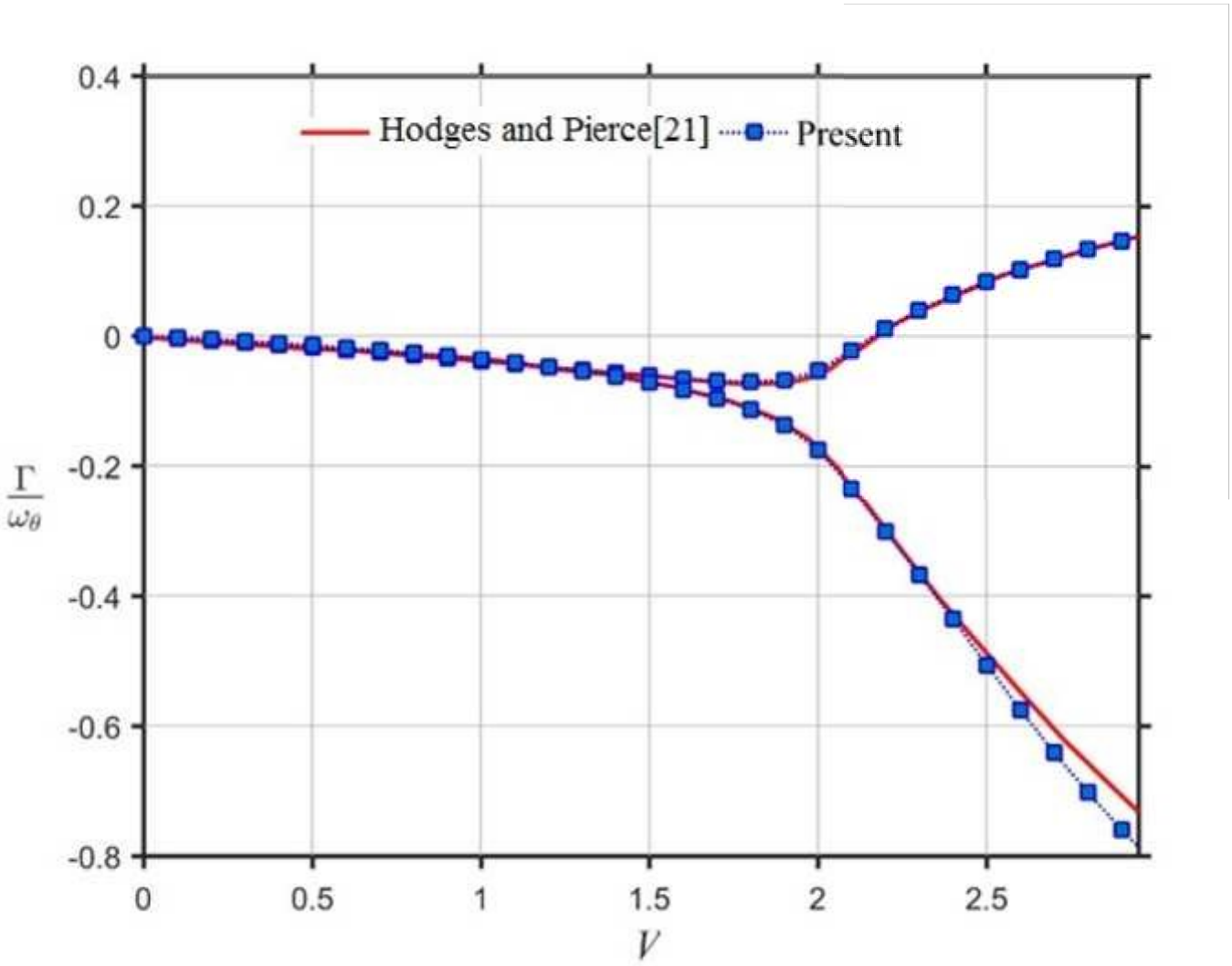

Figure 13. Three-dimensional plot of modal damping versus airspeed for different α-cuts.

Click here to access/download;Figure;figure13.tif

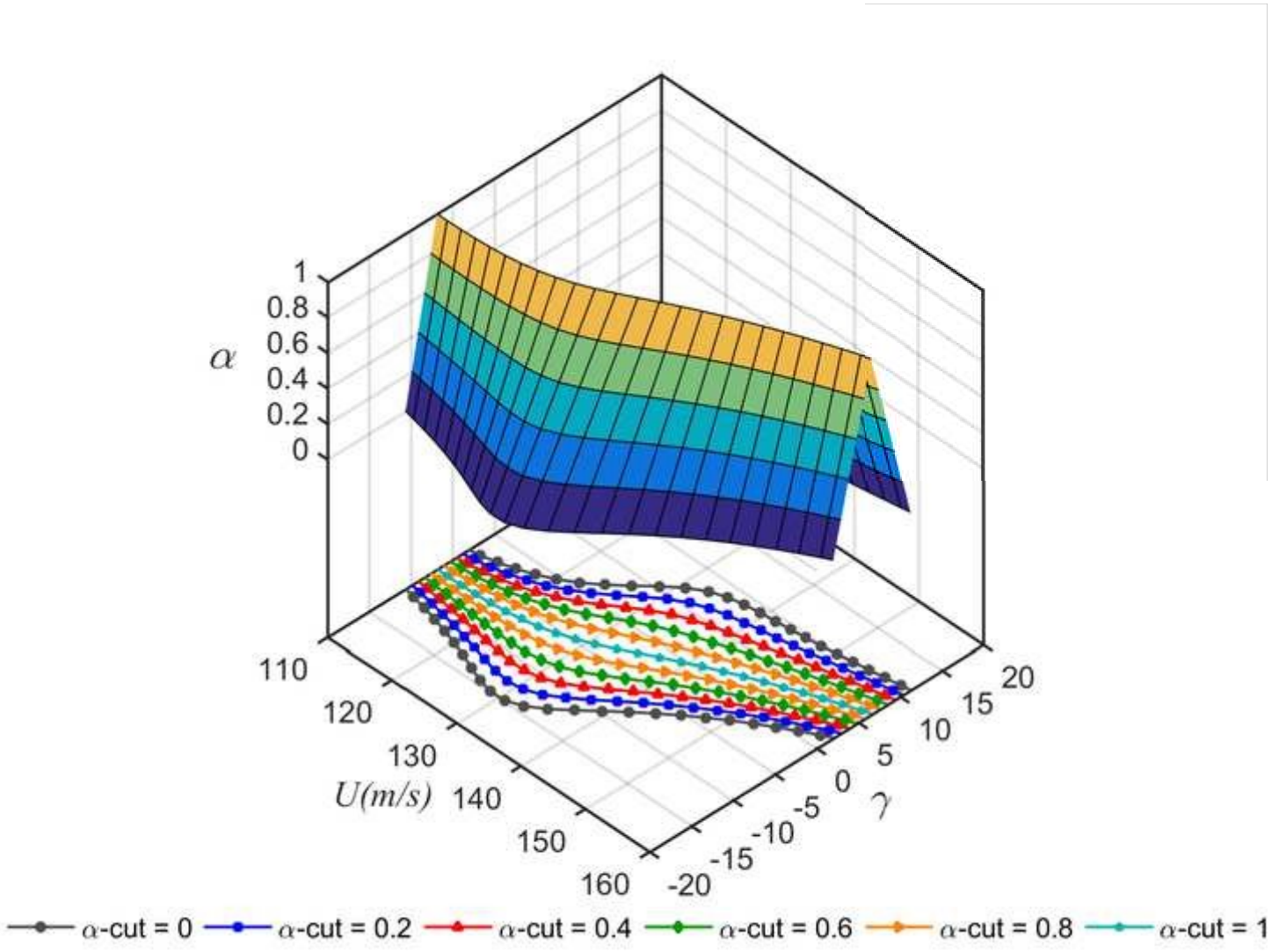

Figure 14. Air speed and flutter speed 3D interference. (a) Case 1, (b) Case 2, (c) Case 3, (d) Case 4,(e) Case 5, (f) Case 6.

Click here to access/download;Figure;figure14a.tif

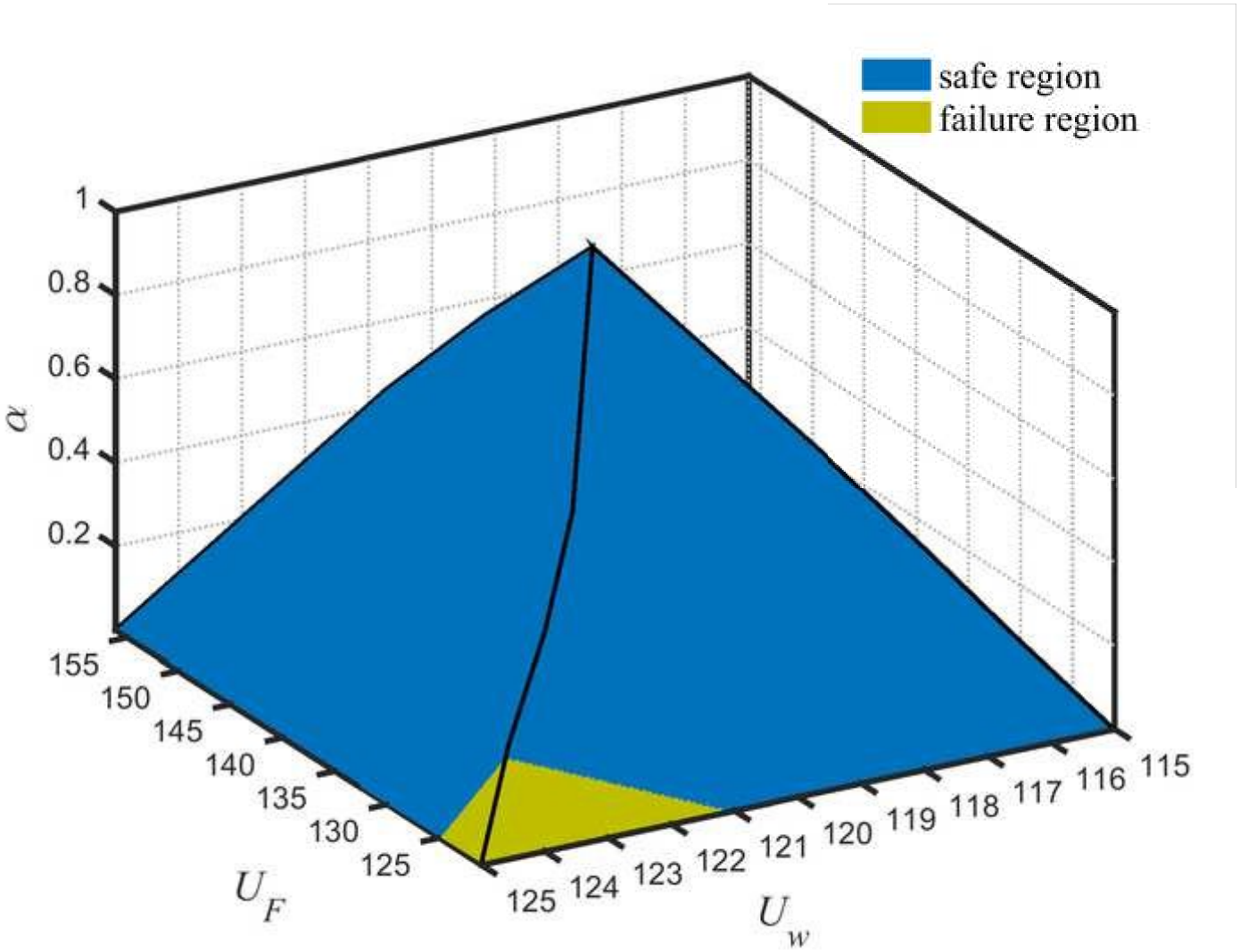

Figure 14. Air speed and flutter speed 3D interference. (a) Case 1, (b) Case 2, (c) Case 3, (d) Case 4,(e) Case 5, (f) Case 6.

Click here to access/download;Figure;figure14b.tif

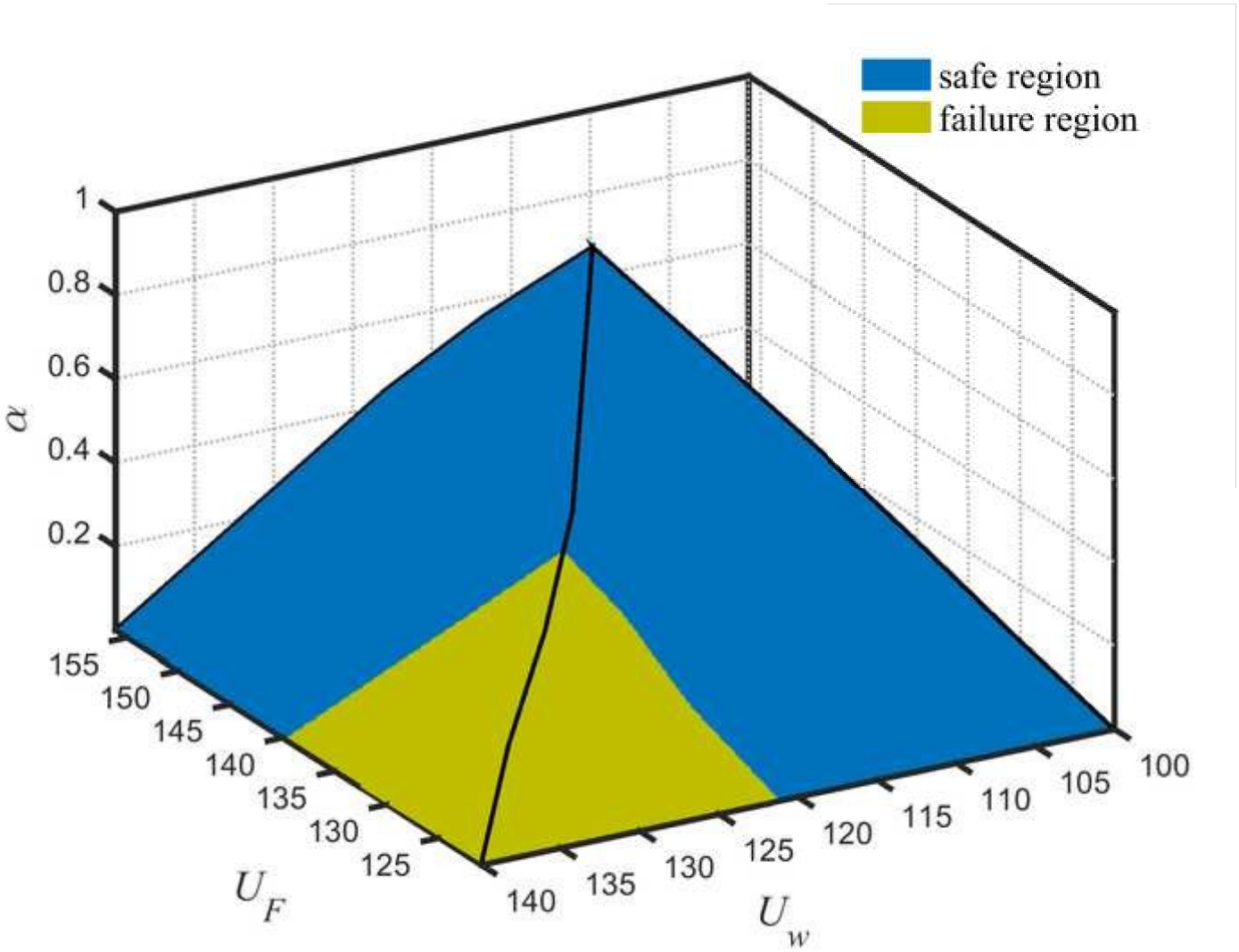

Figure 14. Air speed and flutter speed 3D interference. (a) Case 1, (b) Case 2, (c) Case 3, (d) Case 4,(e) Case 5, (f) Case 6.

Click here to access/download;Figure;figure14c.tif

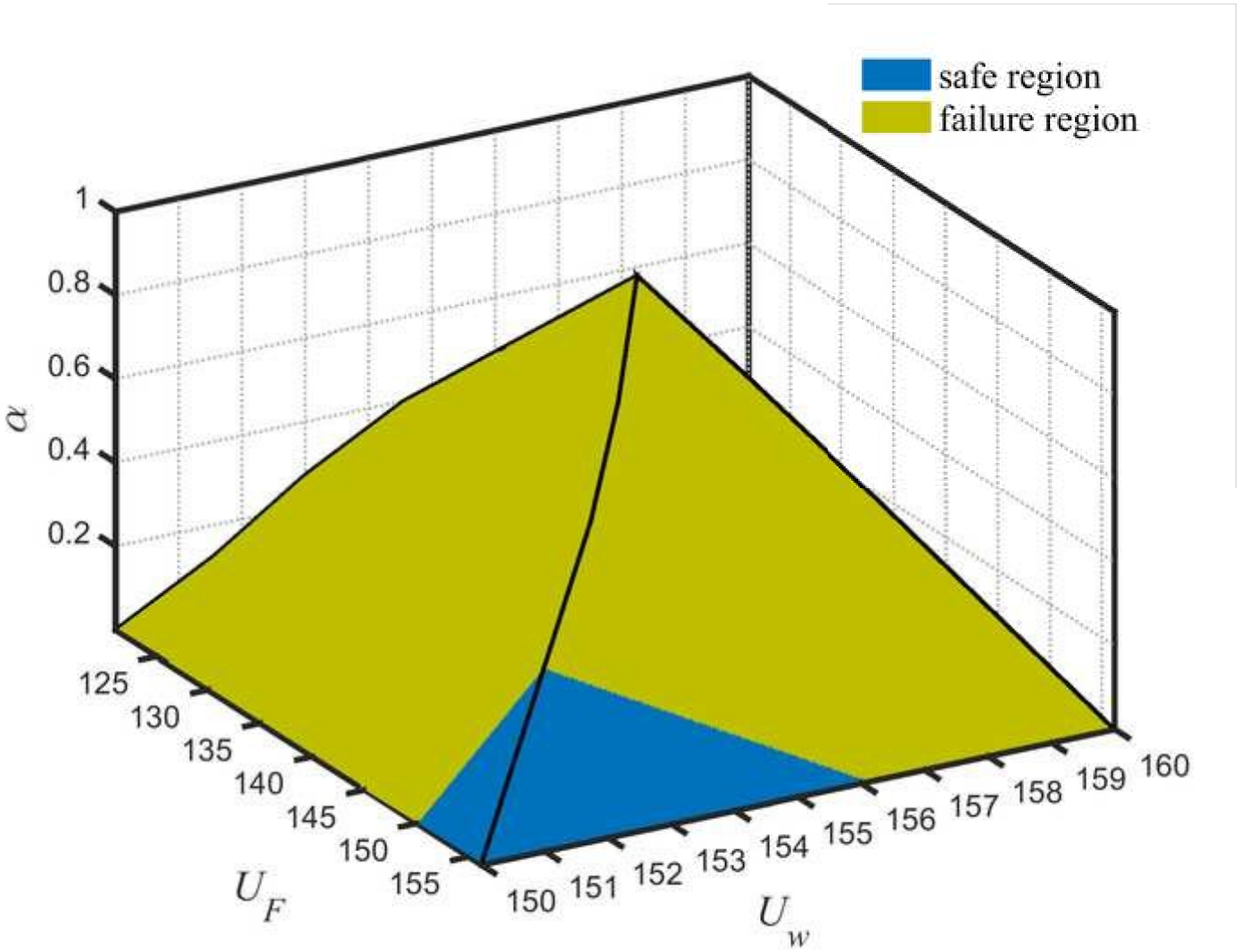

Figure 14. Air speed and flutter speed 3D interference. (a) Case 1, (b) Case 2, (c) Case 3, (d) Case 4,(e) Case 5, (f) Case 6.

Click here to access/download;Figure;figure14d.tif

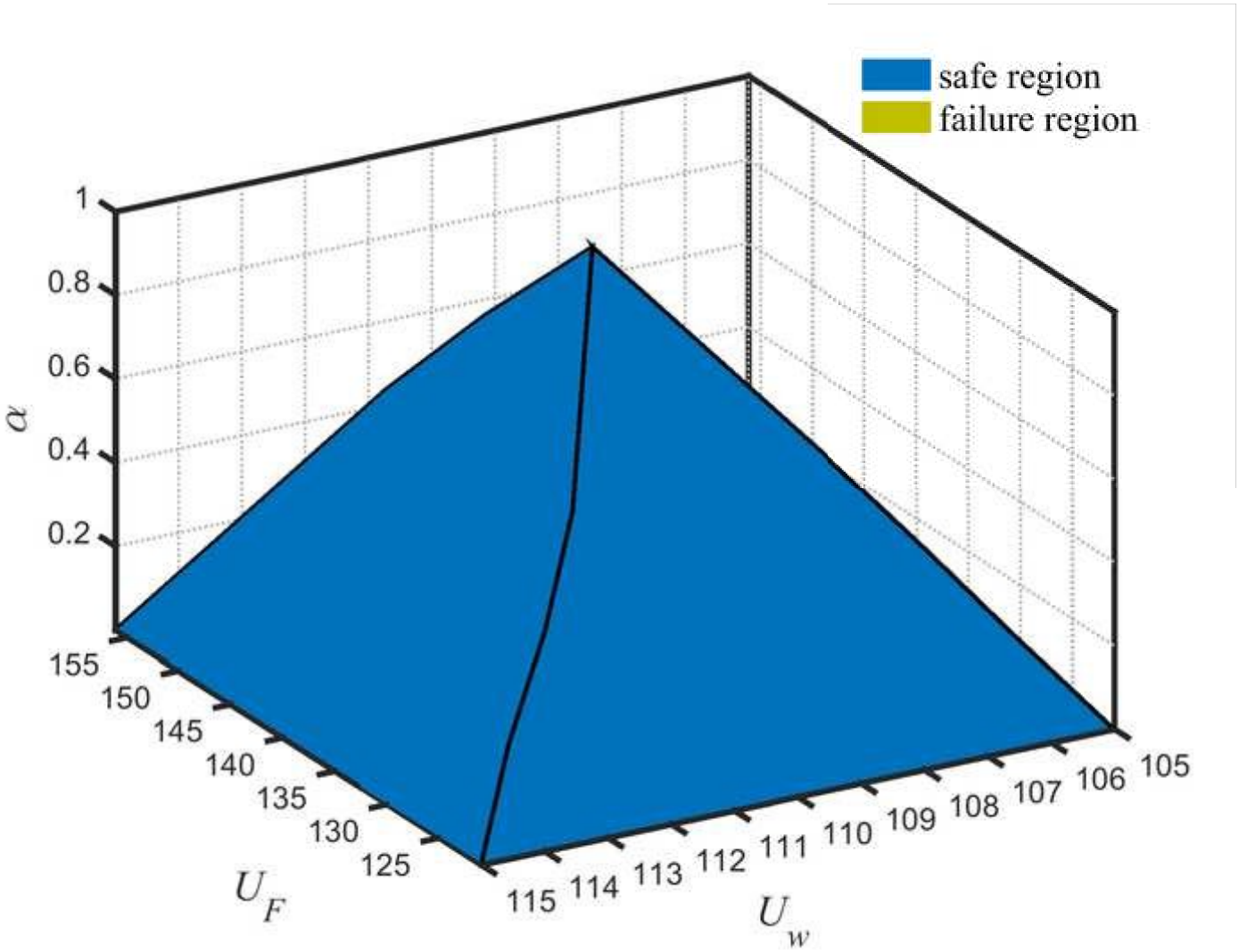

Figure 14. Air speed and flutter speed 3D interference. (a) Case 1, (b) Case 2, (c) Case 3, (d) Case 4,(e) Case 5, (f) Case 6.

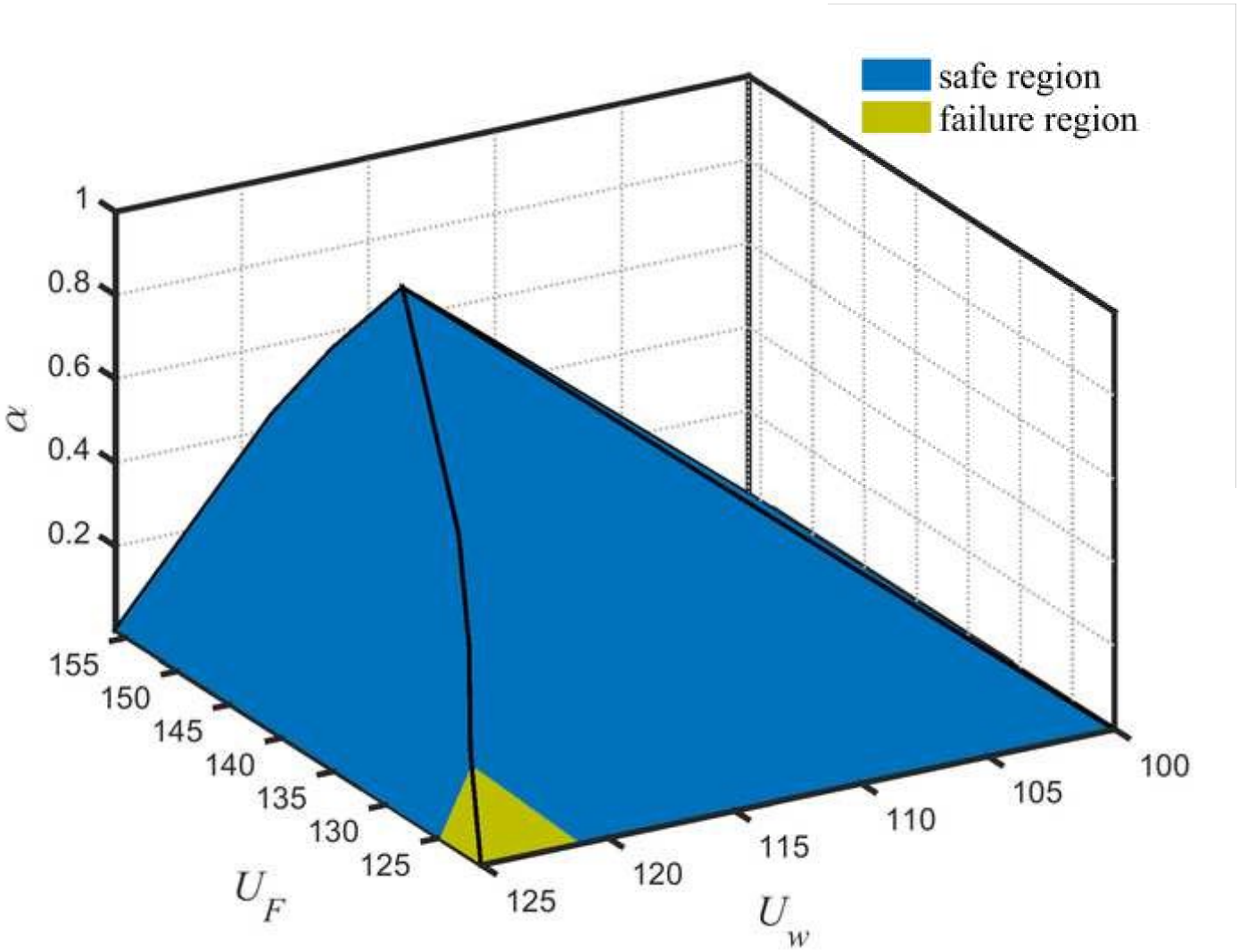

Figure 14. Air speed and flutter speed 3D interference. (a) Case 1, (b) Case 2, (c) Case 3, (d) Case 4,(e) Case 5, (f) Case 6.

Click here to access/download;Figure;figure14f.tif

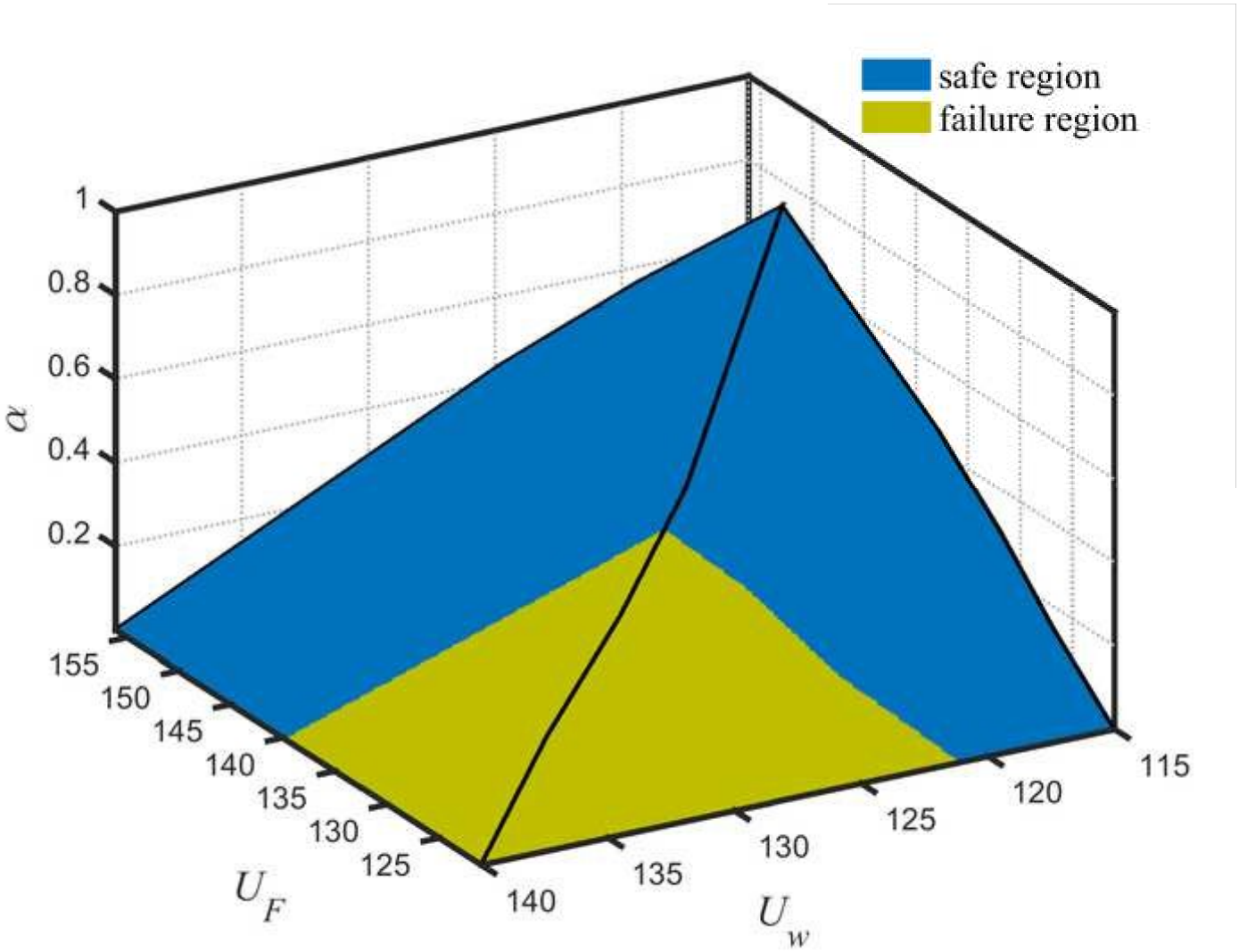

Figure 15. Reliability versus number of α-cuts. (a) Case 1, (b) Case 2, (c) Case 3, (d) Case 4, (e) Case 5, (f) Case 6.

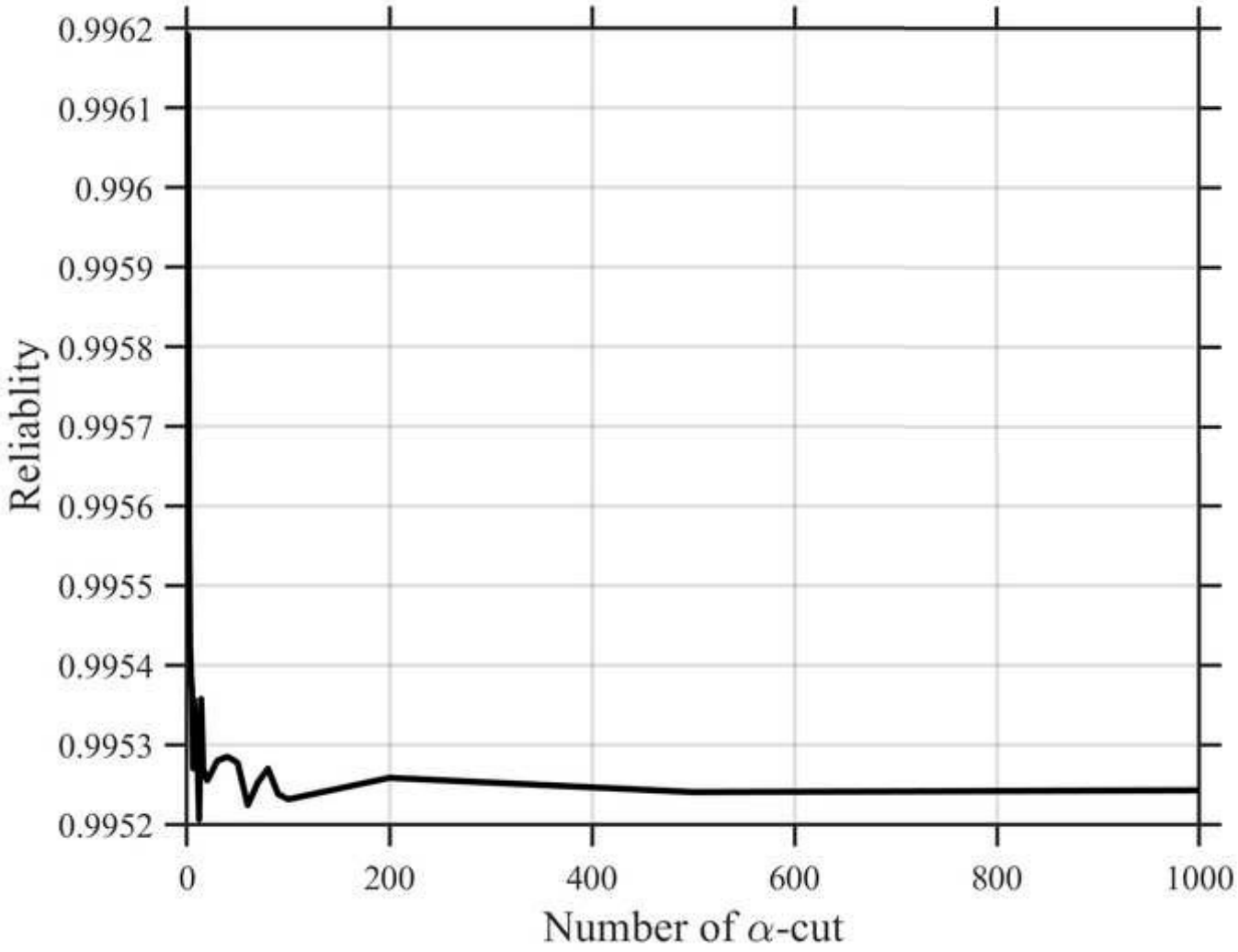

Figure 15. Reliability versus number of α-cuts. (a) Case 1, (b) Case 2, (c) Case 3, (d) Case 4, (e) Case 5, (f) Case 6.

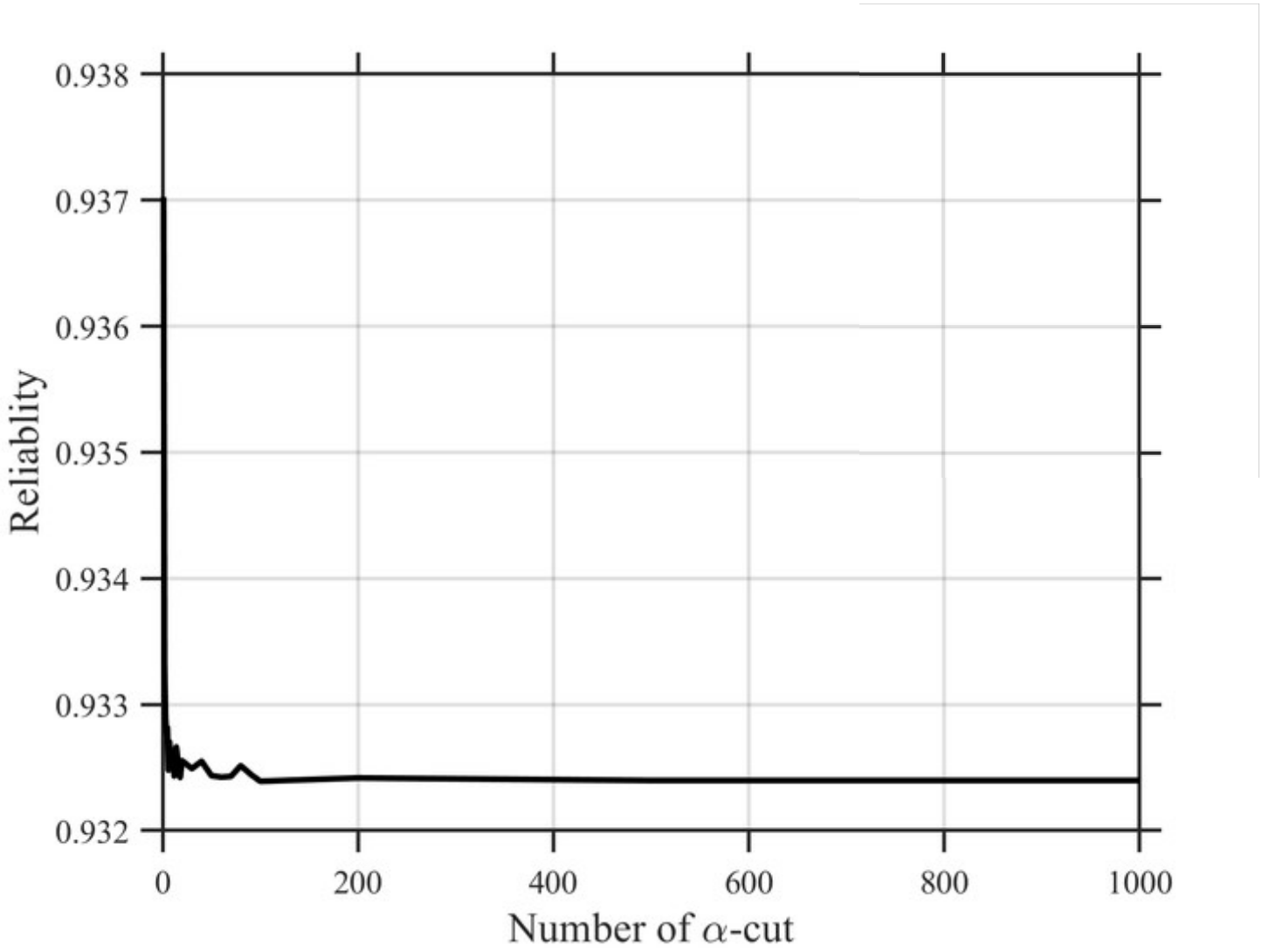

Figure 15. Reliability versus number of α-cuts. (a) Case 1, (b) Case 2, (c) Case 3, (d) Case 4, (e) Case 5, (f) Case 6.

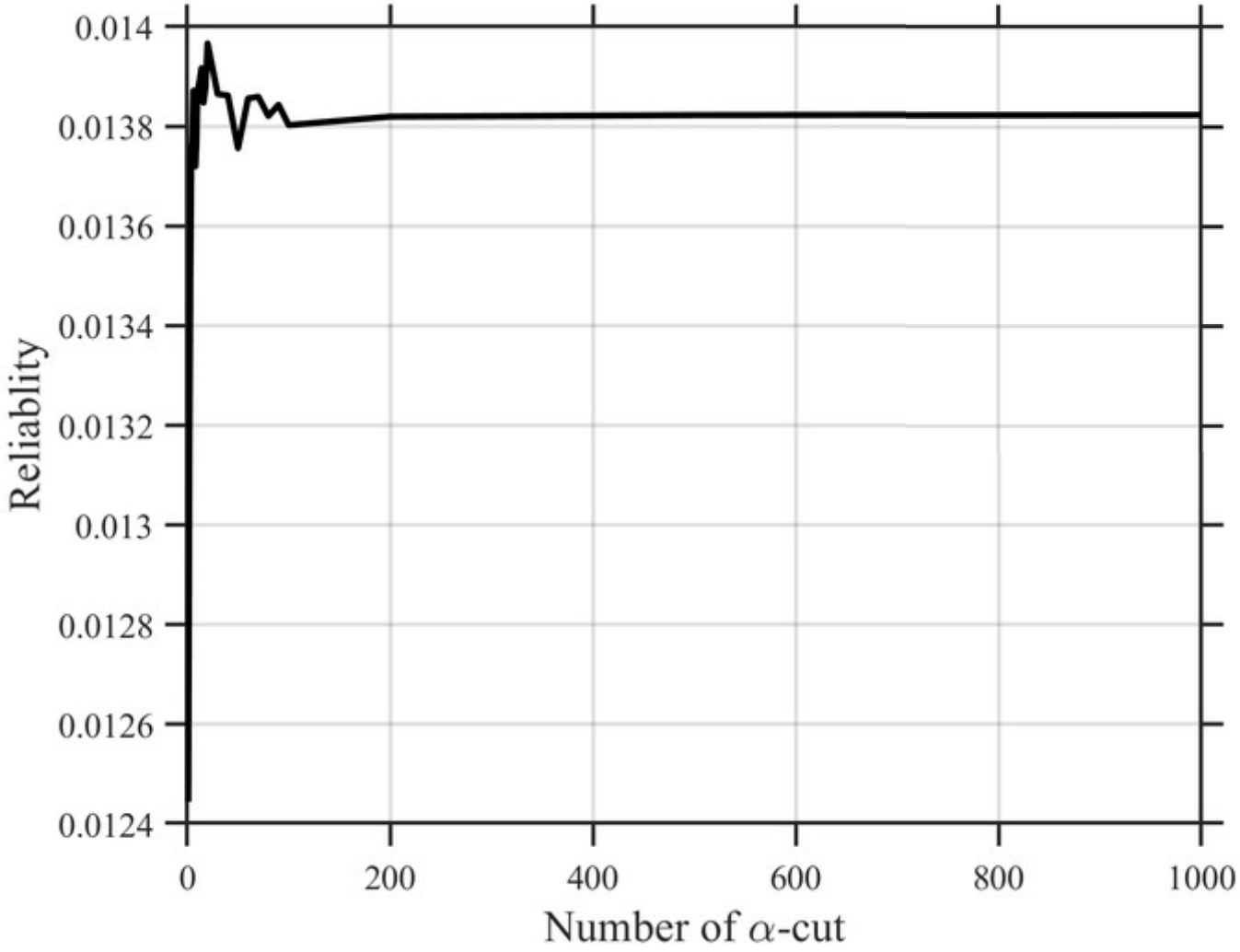

Figure 15. Reliability versus number of α-cuts. (a) Case 1, (b) Case 2, (c) Case 3, (d) Case 4, (e) Case 5, (f) Case 6.

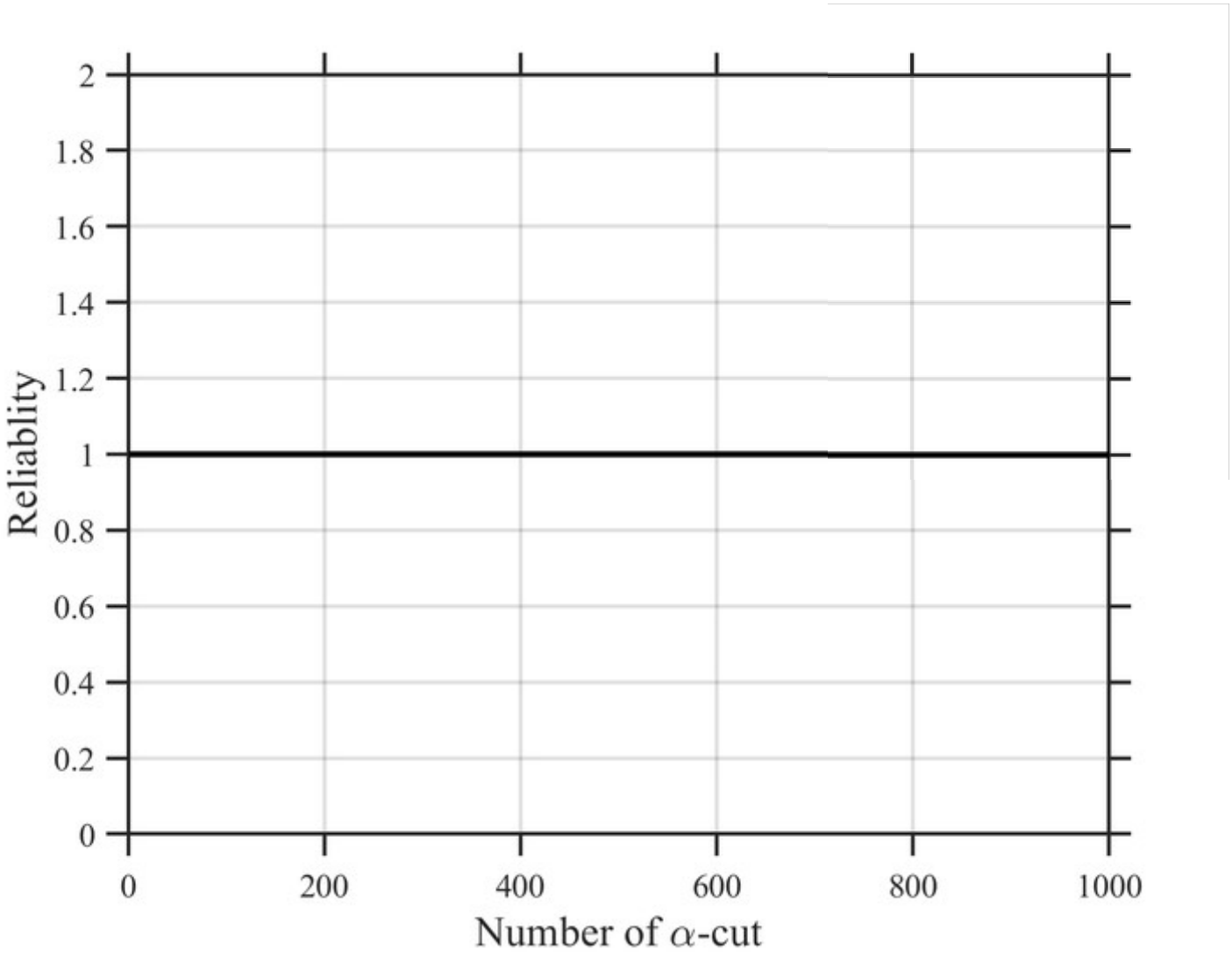

Figure 15. Reliability versus number of α-cuts. (a) Case 1, (b) Case 2, (c) Case 3, (d) Case 4, (e) Case 5, (f) Case 6.

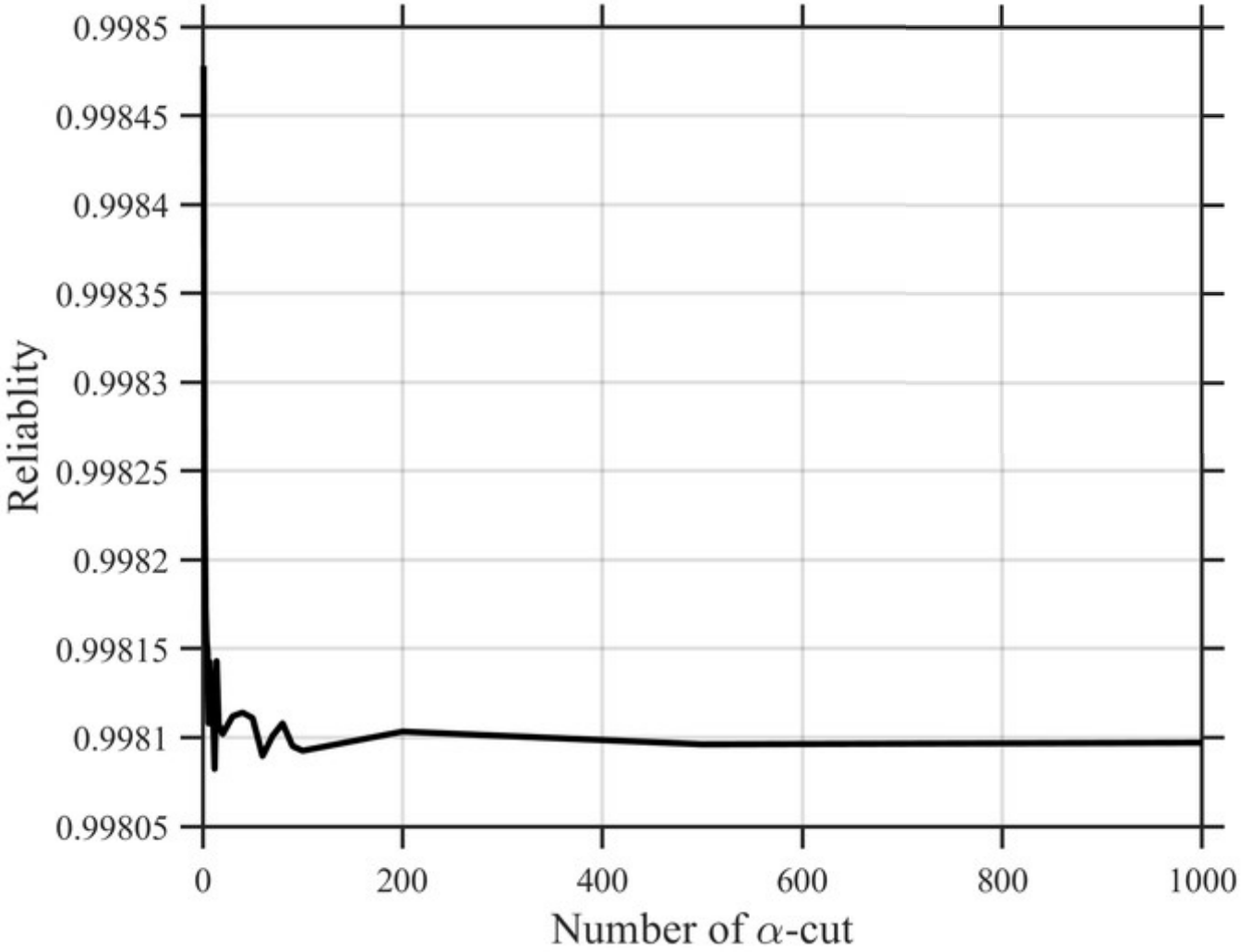

Figure 15. Reliability versus number of α-cuts. (a) Case 1, (b) Case 2, (c) Case 3, (d) Case 4, (e) Case 5, (f) Case 6.

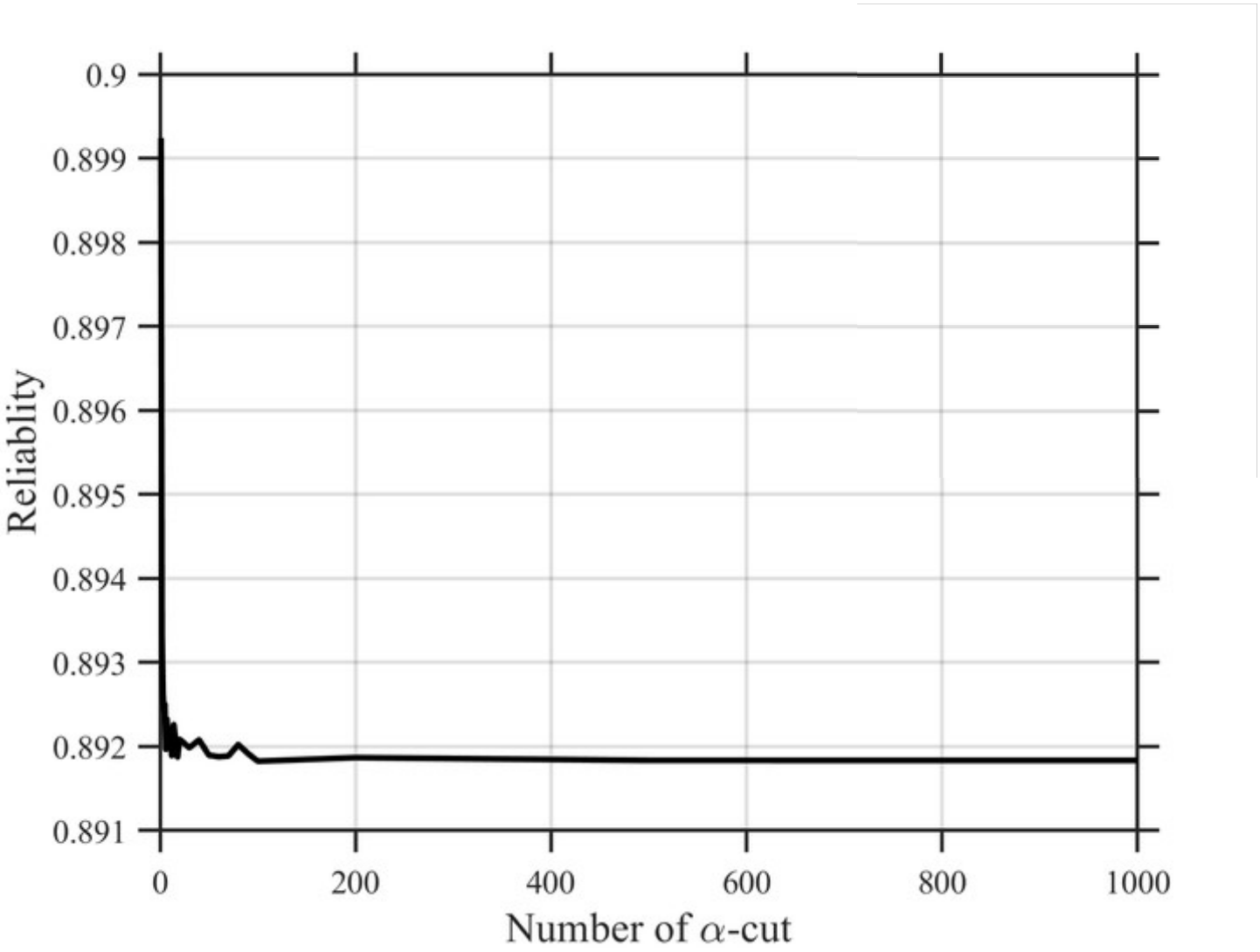

Figure 16. (a) Schematic of the clean wing, and (b) the wing typical section.

Click here to access/download;Figure;Figure16a.tif

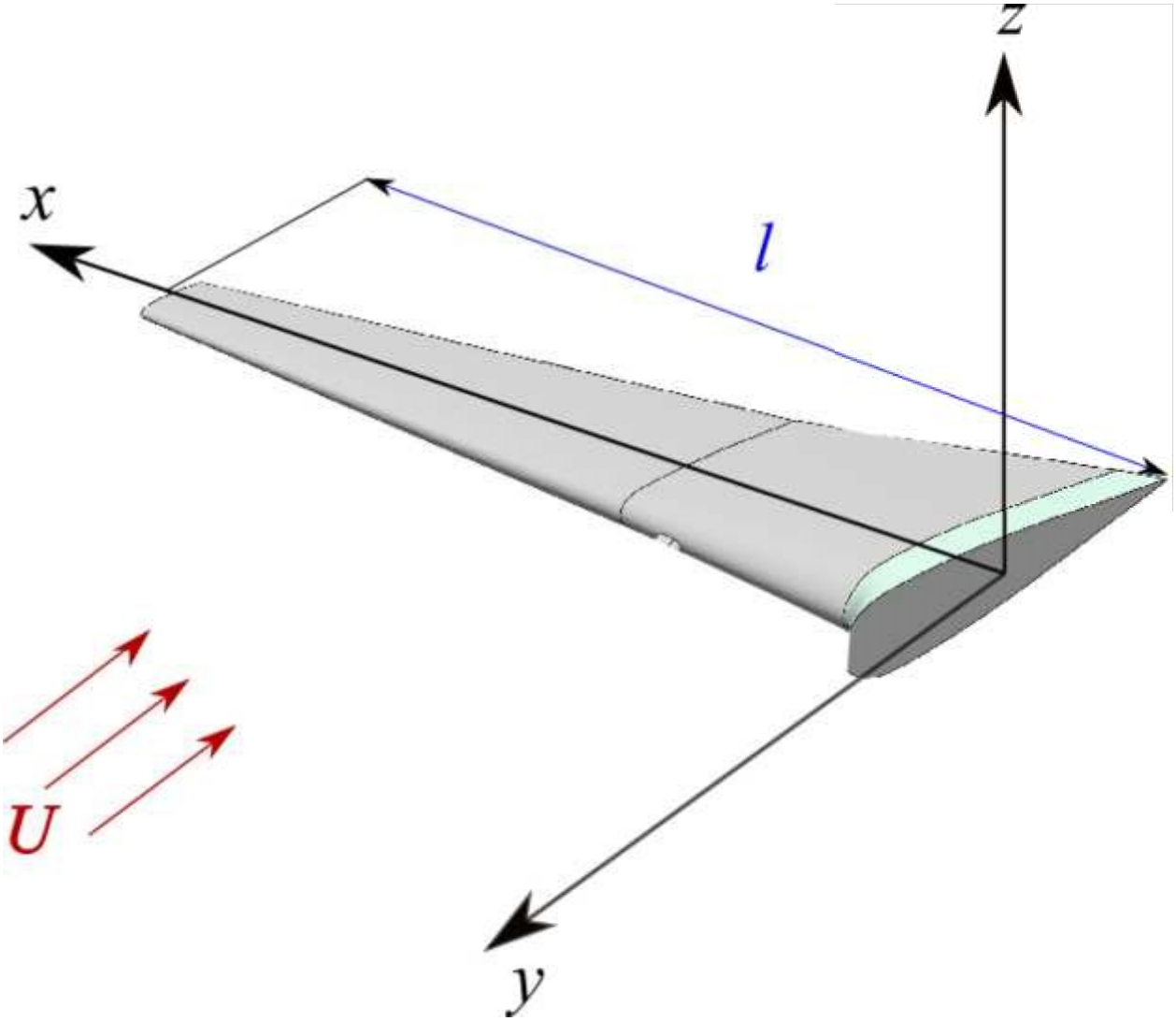

Figure 16. (a) Schematic of the clean wing, and (b) the wing typical section.

Click here to access/download;Figure;Figure16b.tif

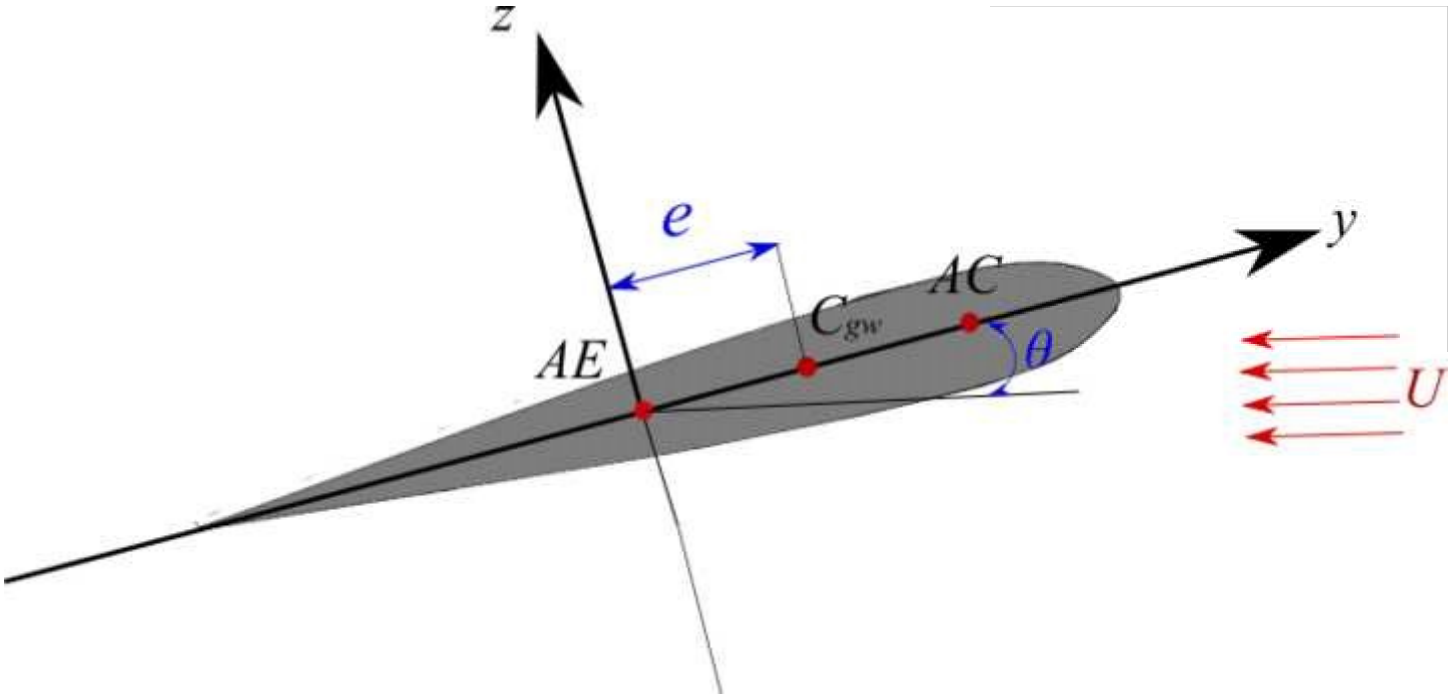

Figure 17. Three-dimensional plot of modal damping versus airspeed for different α-cuts.

Click here to access/download;Figure;figure17.tif

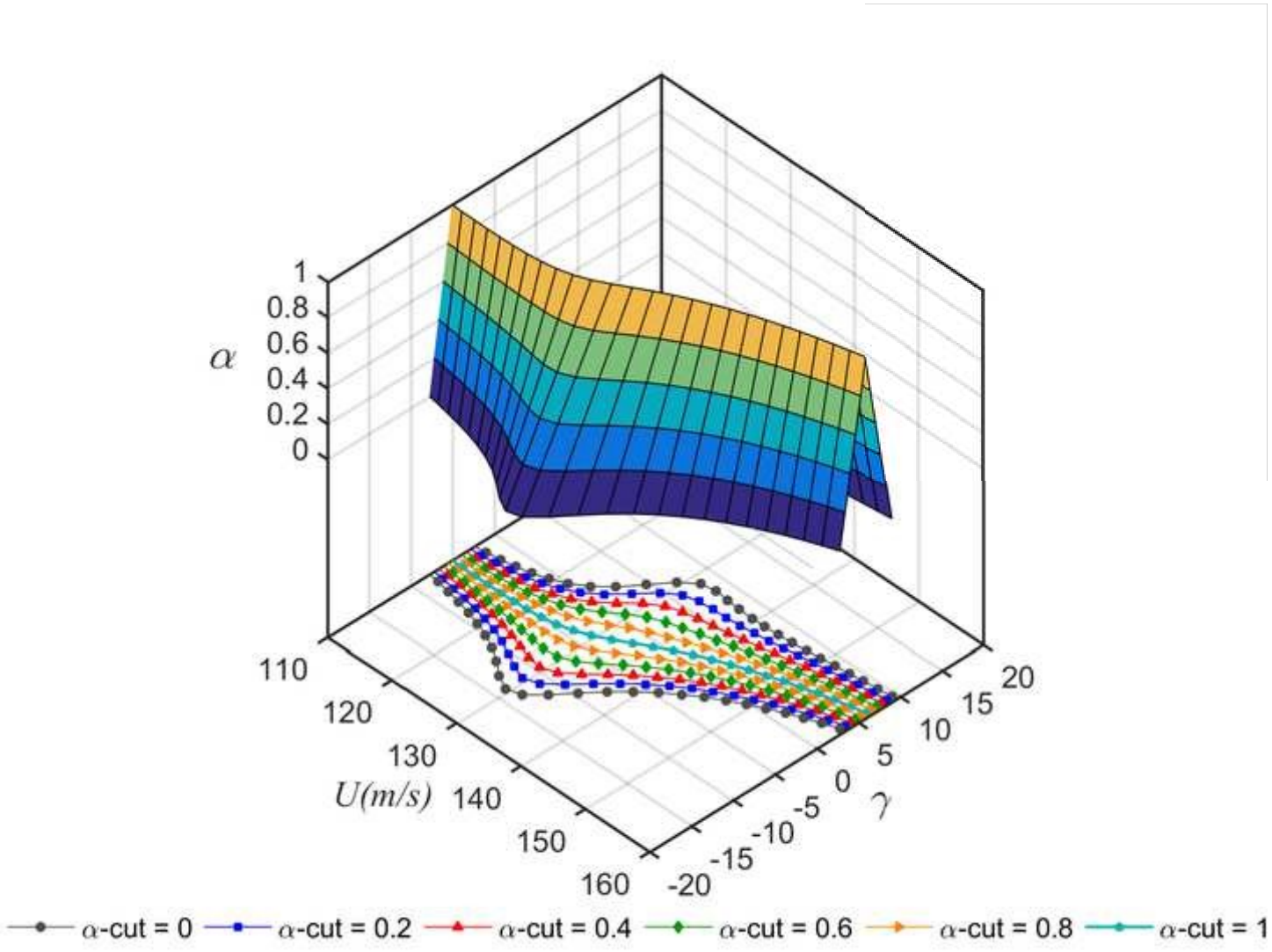

Table 1
Goland wing parameters[6]

Parameters	Value	Unit
EI	9.77×10^{6}	$N.m^2$
GJ	9.890×10^{5}	$N.m^2$
l	6.09	m
x_θ	0.182	m
a	-0.333	
m	35.7187	Kg/m
b	0.9144	m
r	0.457	m
k_θ	8.75×10^{4}	N/m
k_h	6.57×10^{4}	N/m
ρ	1.225	kg/m^3

Table 2
Deterministic flutter speed and frequency

Flutter speed (m/s)	Flutter frequency (rad/s)	Reference
137.09	71.36	Present 3D (Example 2)
140.73	73.21	Present 2D (Example 1)
141.17	72.56	Borello et al. 2D [55]
137.05	75.52	Fazelzadeh et al.3D [47]
137.16	70.69	Goland Exact [53]

Table 3. Number of α-cut and its impact on the accuracy of flutter reliability.

Table 1
Number of α-cut and its impact on the accuracy of flutter reliability

Number of α-Cut	Reliability											
	Case 1		Case 2		Case 3		Case 4		Case 5		Case 6	
	Reliability	Relative Error	Reliability	Relative Error	Reliability	Relative Error	Reliability	Relative Error	Reliability	Relative Error	Reliability	Relative Error
1	0.9962	0.0010	0.9370	0.0050	0.0124	0.0998	1.0000	0.0000	0.9985	0.0004	0.8992	0.0083
2	0.9956	0.0003	0.9333	0.0010	0.0131	0.0501	1.0000	0.0000	0.9982	0.0001	0.8933	0.0017
3	0.9954	0.0002	0.9329	0.0005	0.0135	0.0239	1.0000	0.0000	0.9982	0.0001	0.8926	0.0009
4	0.9954	0.0001	0.9328	0.0004	0.0138	0.0051	1.0000	0.0000	0.9982	0.0001	0.8924	0.0007
5	0.9954	0.0001	0.9328	0.0004	0.0138	0.0041	1.0000	0.0000	0.9981	0.0001	0.8925	0.0007
6	0.9953	0.0000	0.9325	0.0001	0.0139	0.0035	1.0000	0.0000	0.9981	0.0000	0.8920	0.0001
7	0.9954	0.0001	0.9327	0.0003	0.0138	0.0030	1.0000	0.0000	0.9981	0.0000	0.8923	0.0006
8	0.9953	0.0001	0.9326	0.0002	0.0137	0.0075	1.0000	0.0000	0.9981	0.0000	0.8922	0.0004
9	0.9953	0.0001	0.9326	0.0002	0.0138	0.0042	1.0000	0.0000	0.9981	0.0000	0.8921	0.0003
10	0.9953	0.0001	0.9326	0.0002	0.0139	0.0033	1.0000	0.0000	0.9981	0.0000	0.8922	0.0004
12	0.9952	0.0000	0.9324	0.0000	0.0139	0.0048	1.0000	0.0000	0.9981	0.0000	0.8919	0.0001
14	0.9954	0.0001	0.9327	0.0003	0.0139	0.0067	1.0000	0.0000	0.9981	0.0000	0.8923	0.0005
16	0.9953	0.0000	0.9325	0.0002	0.0138	0.0017	1.0000	0.0000	0.9981	0.0000	0.8921	0.0003
18	0.9953	0.0000	0.9324	0.0000	0.0139	0.0039	1.0000	0.0000	0.9981	0.0000	0.8919	0.0000
20	0.9953	0.0000	0.9326	0.0002	0.0140	0.0103	1.0000	0.0000	0.9981	0.0000	0.8921	0.0003
30	0.9953	0.0000	0.9325	0.0001	0.0139	0.0030	1.0000	0.0000	0.9981	0.0000	0.8920	0.0002
40	0.9953	0.0000	0.9325	0.0002	0.0139	0.0028	1.0000	0.0000	0.9981	0.0000	0.8921	0.0003
50	0.9953	0.0000	0.9324	0.0000	0.0138	0.0049	1.0000	0.0000	0.9981	0.0000	0.8919	0.0001
60	0.9952	0.0000	0.9324	0.0000	0.0139	0.0023	1.0000	0.0000	0.9981	0.0000	0.8919	0.0000
70	0.9953	0.0000	0.9324	0.0000	0.0139	0.0026	1.0000	0.0000	0.9981	0.0000	0.8919	0.0001
80	0.9953	0.0000	0.9325	0.0001	0.0138	0.0002	1.0000	0.0000	0.9981	0.0000	0.8920	0.0002
90	0.9952	0.0000	0.9324	0.0001	0.0138	0.0014	1.0000	0.0000	0.9981	0.0000	0.8919	0.0001
100	0.9952	0.0000	0.9324	0.0000	0.0138	0.0015	1.0000	0.0000	0.9981	0.0000	0.8918	0.0000
200	0.9953	0.0000	0.9324	0.0000	0.0138	0.0003	1.0000	0.0000	0.9981	0.0000	0.8919	0.0000
500	0.9952	0.0000	0.9324	0.0000	0.0138	0.0001	1.0000	0.0000	0.9981	0.0000	0.8918	0.0000
1000	0.9952	0.0000	0.9324	0.0000	0.0138	0.0000	1.0000	0.0000	0.9981	0.0000	0.8918	0.0000

Table 4. The reliability of typical section wing flutter speed for α-cut = 1000.

Table 1
The reliability of typical section wing flutter speed for α-cut = 1000

		Wing Typical Section		
	Method (Number of Simulation)	Fuzzy (2001)	Monte Carlo (1000000)	
	Airspeed Membership Function	Reliability	Reliability	error
Case 1	(115,120,125)	99.52 %	99.82%	0.3%
Case 2	(100,120,140)	93.24 %	95.27%	2.1%
Case 3	(150,155,160)	1.382 %	1.42%	2.6%
Case 4	(105,110,115)	100 %	100%	0%
Case 5	(100,120,125)	99.81 %	99.93%	0.1%
Case 6	(115,120,140)	89.18 %	92.41%	3.4%

Table 5. The fuzzy reliability of wing flutter speed.

Table 1
The fuzzy reliability of wing flutter speed

	Airspeed Membership Function	Typical Section	Clean Wing
		Fuzzy Reliability	Fuzzy Reliability
Case 1	(115,120,125)	99.52 %	99.75 %
Case 2	(100,120,140)	93.24 %	92.69 %
Case 3	(150,155,160)	1.382 %	1.28e-3 %
Case 4	(105,110,115)	100 %	100 %
Case 5	(100,120,125)	99.81 %	99.90 %
Case 6	(115,120,140)	89.18 %	88.30 %